Dielectronic recombination of Zn-like W^{44+} from Cu-like W^{45+}

U. I. Safronova, A. S. Safronova, and P. Beiersdorfer

Phys. Rev. A **91**, 062507 — Published 24 June 2015

DOI: 10.1103/PhysRevA.91.062507

Dielectronic recombination of Zn-like W^{44+} from Cu-like W^{45+}

U. I. Safronova* and A. S. Safronova
Physics Department, University of Nevada, Reno, NV 89557

P. Beiersdorfer
Physics Division, Lawrence Livermore National Laboratory, Livermore, CA 94550

Energy levels, radiative transition probabilities, and autoionization rates for [Ar]$3d^{10}4l'nl$ (n=4-12, $l \leq n-1$), [Ar]$3d^{10}5l'nl$ (n=5-8, $l \leq n-1$), and [Ar]$3d^{9}4l'4l''nl$ (n=4-5, $l \leq n-1$) states in Zn-like tungsten (W^{44+}) are calculated using the Hartree-Fock-Relativistic method (COWAN code), the Multi-confiiguration relativistic Hebrew University Lawrence Livermore Atomic Code (HULLAC code), and the relativistic many-body perturbation theory method (RMBPT code). Autoionizing levels above the thresholds [Ar]$3d^{10}4s$ are considered. It is found that configuration mixing [$4sns$ + $4pnp$ + $4dnd$ +4fnf], [$4snp$ + $4pns$ + $4pnd$ + $4dnp$ + $4fns$ + $4fnd$] plays an important role for all atomic characteristics. Branching ratios relative to the first threshold and intensity factors are calculated for satellite lines, and dielectronic recombination (DR) rate coefficients are determined for the first excited odd- and even-parity states. It is shown that the contribution of the highly excited states is very important for the calculation of total DR rates. Contributions to DR rate coefficients from the excited [Ar]$4l'nl$ states with $n \geq 13$ and [Ar]$4l'nl$ states with $n \geq 8$, and additionally from core-excited [Ar]$3d^{9}4l'4l''nl$ states with $n \geq 5$ are estimated by extrapolation of all atomic parameters. The orbital angular momentum quantum number l distribution of the rate coefficients shows two peaks at l=2 and l=5. The total DR rate coefficient is derived as a function of electron temperature. The dielectronic satellite spectra of W^{44+} are important for M-shell diagnostic of very high-temperature laboratory plasmas such as future ITER plasmas.

PACS numbers: PACS: 31.15.ag, 31.15.aj, 31.15.am, 31.15.vj

I. INTRODUCTION

Recently, Spruck *et al.* [1] presented experimentally measured and theoretically calculated rate coefficients for the electron-ion recombination of W^{18+} ([Kr]$4d^{10}4f^{10}$) forming W^{17+}. At low electron-ion collision energies, the merged-beam rate coefficient is dominated by strong, mutually overlapping recombination resonances. In the temperature range where the fractional abundance of W^{18+} is expected to peak in a fusion plasma, the experimentally derived Maxwellian recombination rate coefficient was 5 to 10 times larger than that which is currently recommended for plasma modeling. The complexity of the atomic structure of the open $4f$ system under study makes the theoretical calculations extremely demanding. Nevertheless, the results of the presented Breit-Wigner partitioned dielectronic recombination calculations agreed reasonably well with the experimental findings. This also gives confidence in the ability of the theory to generate sufficiently accurate atomic data for the plasma modeling of other complex ions [1].

Accurate determinations of dielectronic recombination (DR) rate coefficients are crucial for determining the correct charge balance in a high temperature plasma, and thus for determining the correct energy balance, which is of particularly importance in laser-produced Z-pinch plasmas formed by high-Z ions seen as tungsten, as discussed in Ref. [2]. Different computer codes use different approaches in the treatment of DR and, therefore, may predict very different ionization equilibria, as documented in a series of code comparison workshops delineated in Refs. [3, 4]. Correct knowledge of the ionization balance at a given electron temperature is also required for determing transport parameters in magnetic fusion plasmas. Here, transport changes the ionization balance because ions move radially from hotter to colder and from colder to hotter plasma regions, as discussed in Refs.[5, 6]. Thus, deviations from the transport-free ionization equilibrium calculations observed experimentally can be a direct measure of transport. Moreover, spectral feature produced by DR are of great diagnostic utility provided that the intensity of these features is correctly calculated, as also discussed in Refs.[5, 6]. Calculations of DR parameters specifically for tungsten ions has increased in importance with the decision to use tungsten in plasma-facing component on ITER (latin 'the way') tokamak under construction in France. ITER plasmas will contain an abundance of radiating tungsten. In fact, this radiation will be monitored by various spectrometers covering different wavelength bands and plasma regions Ref. [7–9].

Dielectronic recombination of Br-Like tungsten ions was investigated in Ref. [10]. Theoretical calculations were made for dielectronic recombination (DR) rate coefficients of Br-like tungsten ions using the relativistic Flexible Atomic Code (FAC) from 1 eV to 50 keV [10]. DR coefficients were given theoretically for several highly charged tungsten ions in Ref [11]. As $4p$ open sub-shell

*Electronic address: ulyanas@unr.edu

ions, Ga-, Ge-, As-, Br-, Kr-like ions were considered. The Rb-like ion was further considered as a $4d$ open sub-shell ion. Theoretical calculations were carried out using FAC [11]. Polarization of the $nf \rightarrow 3d$ (n = 4, 5, 6) xrays from tungsten ions following electron-impact excitation and dielectronic recombination processes was studied recently in Ref. [12]. Electron-impact excitation and resonant electron capture cross sections to the specific magnetic sublevels as well as the polarization of the strong $nf \rightarrow 3d$ (n = 4, 5, 6) xrays emitted from Ni-like through Ge-like tungsten ions were investigated systematically by using a fully relativistic distorted-wave method. It was found that the degrees of xray polarization following electron-impact excitation and dielectronic recombination were totally different [12].

Dielectronic recombination of xenonlike tungsten ions was investigated by Schippers *et al.* [13, 14] experimentally at a heavy-ion storage ring. A merged-beams method was employed for obtaining absolute rate coefficients for electron-ion recombination in the collision-energy range 0–140 eV [13]. Theoretically, DR of xenonlike W^{20+} with an almost half-open $4f$ shell ($4d^{10}4f^8$) was investigated by Badnell *et al.* [15]. These authors carried out DR calculations with the atomic physics code AUTOSTRUCTURE which included all significant single-electron promotions. Their intermediate-coupling (IC) results were more than a factor of 4 larger than the LS-coupling ones at 1 eV but still lay a factor of 3 below experiment here [15]. A statistical theory of resonant multielectron recombination based on properties of chaotic eigenstates was developed by Dzuba *et al.* [16]. These authors underlined that in many cases individual resonances were not resolved experimentally (since the interval between them is small, e.g., $\leq$ 1 meV, possibly even smaller than their radiative widths); therefore, statistical theory should correctly describe the experimental data. They performed numerical calculations of the recombination cross sections for tungsten ions W^{q+}, q = 18–25 [16].

The theoretical study of the DR of Rh-like Gd and W was presented in Ref. [17]. Energy levels, radiative transition probabilities, and autoionization rates of Pd-like gadolinium and tungsten were calculated using the FAC code. The contributions from resonant and nonresonant radiative stabilizing transitions to the total rate coefficients were discussed [17]. The DR of the Er-like ion W^{6+} proceeds via electron capture into the intermediate autoionizing states of the Tm-like ion W^{5+} followed by the radiative decay to singly-excited bound states was studied in Ref. [18]. Relativistic atomic data for Cu-like tungsten were evaluated in Ref. [19]. Contributions from the autoionizing doubly excited $[\mathrm{Ne}]3s^23p^63d^94l'nl$, $[\mathrm{Ne}]3s^23p^53d^{10}4l'nl$, and $[\mathrm{Ne}]3s^23p^63d^95l'nl$ states (with n up to 500), which are particulary important for calculating total DR rates, were estimated. Synthetic dielectronic satellite spectra from Cu-like W were simulated in a broad spectral range from 3 to 70 Å. Excitation energies, radiative and autoionization rates, dielectronic satellite lines, and dielectronic recombination rates for excited states of Yb-like W^{4+} and Ag-like W^{27+} ions were given in Refs. [20, 21]. Dielectronic satellite lines and dielectronic recombination rates for high ionization stages such as Na-like W from Ne-like W and Mg-like W from Na-like W were presented by Safronova *et al.* in Refs. [22–24]. The relativistic many-body perturbation theory method (RMBPT code), the Multi-confiiguration relativistic Hebrew University Lawrence Livermore Atomic Code (HULLAC code), and the Hartree-Fock-Relativistic method (COWAN code) were used to perform a large-scale calculation of atomic parameters (excitation energies, radiative and autoionization rates) to evaluate DR rate coefficients and to build synthetic satellite spectra in Refs. [18, 20–24]. Additional theoretical calculations of the DR of Ne-, Ar-, Co-, Ni-, Cu-, Y- like tungsten were presented in Refs. [25–33].

Recently, the atomic structure and spectra of ten tungsten ions were calculated by Clementson *et al.* [34] using FAC. The calculations yield energy levels, radiative lifetimes, spectral line positions, transition probability rates, and oscillator strengths for the tungsten ions isoelectronic to germanium,W^{42+}, through vanadium, W^{51+}. Oscillator strengths and transition probabilities for the W^{44+} ion were evaluated by Spencer *et al.* [35]. The calculations were performed with the configuration interaction CIV3 program with the inclusion of relativistic effects achieved through the use of the Breit-Pauli approximation. A detailed study using fully relativistic distorted wave theory for electron impact excitation of Zn-like through Co-like tungsten ions for a wide range of incident electron energies was presented by Das *et al.* [36]. Hu *et al.* [37] reported a large *ab initio* calculation for the $4s^24s4p$ transitions in the Zinc-like sequence, using the Multi-configuration Dirac-Hartree-Fock method. Spectroscopic analysis and modeling of tungsten experiment from electron beam trap and Z-pinch plasmas was reported by Osborne *et al.* [38]. In particular, Co-, Ni-, Zn-, Cu-, Ga-, and Ge-like tungsten transitions were included in HULLAC calculations used to interpret spectra. A comprehensive theoretical study of atomic characteristics of eight isoelectronic sequences of tungsten ions in a broad range of wavelengths and transitions was reported in Ref. [39]. In particular, excitation energies, oscillator strengths and transition probabilities were calculated for $nln'l'$ transitions in W^{70+}, W^{69+}, W^{62+}, W^{61+}, W^{54+}, W^{44+}, W^{27+}, and W^{4+} ions using the RMBPT method [39]. Transition rates, oscillator strengths and line strengths were calculated for electric-dipole (E1) transitions between even-parity $4s2$, $4p2$, $4s4d$, $4d2$, $4p4f$ and $4f2$ states and odd-parity $4s4p$, $4s4f$, $4p4d$ and $4d4f$ states in Zn-like ions with the nuclear charge ranging from Z = 32 to 100 [40]. Relativistic many-body perturbation theory, including the Breit interaction, was used to evaluate retarded E1 matrix elements in length and velocity forms. A large-scale relativistic configuration-interaction approach applied to the $4s^24s4p$ transition energies and E1 rates for Zn-like ions was presented by

Chen and Cheng [41]. B-spline basis functions were used for these large-scale calculations. QED corrections to the excitation energies were also calculated [41]. Earlier theoretical calculations of energies, wavelengths, oscillator strengths and transition rates of Zn-like ions were presented in Refs. [42–55].

In the present paper, we evaluate energy levels, radiative transition probabilities, and autoionization rates for [Ar]$3d^{10}4l'nl$ (n=4-12, $l \leq n-1$), [Ar]$3d^{10}5l'nl$ (n=5-8, $l \leq n-1$), and [Ar]$3d^{9}4l'4l''nl$ (n=4-5, $l \leq n-1$) states in Zn-like tungsten (W^{44+}) to build synthetic spectra of the Zn-like W^{44+} ion. The DR rate coefficients are determined for the singly excited [Ar]$3d^{10}4l'nl$ (n=4-12, $l \leq n-1$), [Ar]$3d^{10}5l'nl$ (n=5-8, $l \leq n-1$), and as well as doubly excited non-autoionizing [Ar]$3d^{9}4l'4l''nl$ (n=4, $l \leq n-1$) states in Zn-like W^{44+} ion. Contributions from these states (with n up to 500), which are particulary important for calculating total DR rates, are estimated. Energy levels, radiative transition probabilities, and autoionization rates for those states are calculated using the COWAN, HULLAC, and RMBPT codes. These three codes allow us to check the accuracy of our calculations and to achieve confidence that our predictions are reliable. We present the state-selective DR rate coefficients to excited states of Cu-like tungsten as well as the total DR rate coefficients as a function of electron temperature. In addition, we present a detailed comparison of our theoretical calculations with the recommended data published by Kramida and Shirai [56], which is another test the accuracy of our results. Below, we omit the core [Ar] = $1s^22s^22p^63s^23p^6$ from the configuration notation.

II. ENERGY LEVELS, TRANSITION PROBABILITIES, AND AUTOIONIZATION RATES

Detailed calculations of dielectronic recombination parameters should include the determination of such characteristics as energies, radiative transition probabilities, and autoionization rates for atomic states in the recombined ion. Therefore, we calculated the energies, radiative and autoionization rates for the intermediate states $3d^{10}4l'nl$ (n=4-12, $l \leq n-1$), $3d^{10}5l'nl$ (n=5-8, $l \leq n-1$), and $3d^{9}4l'4l''nl$ (n=4-5, $l \leq n-1$) states in Zn-like tungsten (W^{44+}) ion.

The complete list includes 204 $3d^{10}4l'nl$ configurations, 198 $3d^{10}5l'nl$ configurations, and 63 $3d^{9}4l'4l''nl$ configurations (for a total of 9105 levels). Due to computational issues, the calculation of the DR parameters involving the $3d^{10}4l'nl$ and $3d^{9}4l'4l''nl$ states was performed by including states only with $n \leq 8$ and $n \leq 5$, respectively.

The resulting list of levels included in the set of $3d^{10}4l'nl$ configurations with n=4-12 consists of 1074 even-parity and 1115 odd-parity states, which give rise to 669,968 transitions. The set of $3d^{10}5l'nl$ (n=5-8) configurations contains 970 even-parity and 1012 odd-parity states, which give rise to 597,654 transitions. The set of $3d^{9}4l'4l''nl$ (n=4-5) configurations contains 2318 even-parity and 2616 odd-parity states. These lead to 722,794 transitions.

Our large-scale calculations of atomic properties are based on three atomic computer codes: the Multi-Configuration Hartree-Fock (MCHF) code developed by Cowan (in the following we will refer to it as the "COWAN" code) [57], the multi-configuration relativistic Hebrew University Lawrence Livermore Atomic Code (the HULLAC code)[58], and the Relativistic Many-Body Perturbation Theory code (the RMBPT code). The RMBPT method was described in detail in [59, 60]. These three codes allow us to check the accuracy of our calculations, and agreement between the results from each code provide confidence that our predictions are reliable.

We use the version of the Cowan code available in [61]. This version allows us to take into account a large number of configurations (up to 100 odd- and 100 even-parity configurations). The scaling of electrostatic integrals in the Cowan code allows us to correct for correlation effects and to obtain good agreement with experimental energies. We employed a single scaling factor (0.85) for all electrostatic integrals.

In the HULLAC code, the intermediate-coupling detailed level energies are calculated using the relativistic version of the parametric potential method, including configuration mixing. The autoionization rate coefficients are calculated in the distorted-wave approximation, implementing the highly efficient factorization-interpolation method.

The RMBPT code, including the Breit interaction, is used to evaluate energies and transition rates for multipole transitions. This method is based on the relativistic many-body perturbation theory, agrees with Multi-Configuration Dirac-Fock (MCDF) calculations in lowest-order, includes all second-order correlation corrections, and includes corrections from negative energy states. First-order perturbation theory is used to obtain intermediate-coupling coefficients, and second-order RMBPT is used to determine the matrix elements. The RMBPT code is an *ab-initio* code without the scaling of electrostatic integrals as used in the Cowan code and without any parametric potentials as employed in the HULLAC code. The RMBPT code is more complicated to use than the COWAN and HULLAC codes when including the second-order correlation contribution.

The results of our calculations of energies and transition rates are presented in Tables I - III. In Table I, the energies for the $3d^{10}4l'4l$ excited states of Zn-like tungsten are given. We compare our results obtained using all three codes. The differences between the results are about 0.1–0.5%, except for some levels (see the $3d^{10}4s4p\ ^3P_0,\ ^3P_1$ levels, for example) where the differences are as much as 1–2%. It should be noted that we list in this table both LS (left column for "COWAN" results) and jj (columns with "HULLAC" and "RMBPT"

TABLE I: Energies (10^3 cm^{-1}) of the $3d^{10}4l4l'$ excited states of Zn-like tungsten, obtained using the COWAN, HULLAC, and RMBPT codes. Our results are compared with compiled data from Kramida and Shirai [56]. Designations: $3d^{10}4l4l' = 4l4l'$.

Level	E (10^3 cm^{-1})				Level	E (10^3 cm^{-1})		
	COWAN	HULLAC	RMBPT	[56]		COWAN	HULLAC	RMBPT
$4s^2\ ^1S_0$	0.00	0.00	0.00	0	$4d^2\ ^3P_0$	5650.78	5710.36	5690.10
$4s4p\ ^3P_0$	683.60	699.44	696.87	695	$4d^2\ ^3F_3$	5741.34	5773.33	5762.15
$4s4p\ ^3P_1$	735.02	758.57	752.29	752.56	$4d^2\ ^1G_4$	5755.41	5783.19	5772.64
$4s4p\ ^3P_2$	1517.59	1503.31	1505.33	1494.4	$4d^2\ ^3P_2$	5769.90	5806.97	5794.10
$4p^2\ ^3P_0$	1559.16	1609.01	1589.47		$4d^2\ ^3P_1$	5792.65	5839.52	5823.70
$4s4p\ ^1P_1$	1642.86	1651.01	1641.86	1641.23	$4d^2\ ^3F_4$	5873.00	5881.26	5876.05
$4p^2\ ^3P_1$	2349.37	2359.67	2347.79		$4p4f\ ^1F_3$	5881.40	5894.95	5884.14
$4p^2\ ^1D_2$	2361.26	2369.82	2359.81		$4p4f\ ^3F_2$	5902.55	5923.60	5910.81
$4s4d\ ^3D_1$	2766.54	2789.67	2781.70		$4p4f\ ^3D_1$	5920.79	5939.78	5927.04
$4s4d\ ^3D_2$	2792.45	2818.35	2809.01	2809.5	$4p4f\ ^3G_4$	5926.52	5955.14	5926.61
$4s4d\ ^3D_3$	2942.08	2958.33	2952.43		$4p4f\ ^3G_5$	5930.59	5936.62	5938.83
$4s4d\ ^1D_2$	2987.13	3004.47	2997.79	2998.5	$4p4f\ ^3D_3$	5942.64	5951.43	5941.01
$4p^2\ ^3P_2$	3226.26	3225.28	3211.11		$4d^2\ ^3P_2$	5945.49	5970.17	5958.40
$4p^2\ ^1S_0$	3268.28	3262.86	3251.48		$4d^2\ ^1S_0$	6038.24	6093.48	6074.39
$4p4d\ ^3F_2$	3493.80	3527.17	3516.41		$4p4f\ ^1D_2$	6038.85	6074.68	6055.56
$4p4d\ ^3D_1$	3611.47	3671.84	3649.83		$4p4f\ ^1G_4$	6051.70	6099.01	6072.96
$4p4d\ ^3P_2$	3734.24	3775.68	3759.91		$4d4f\ ^3H_4$	7029.23	7065.53	7054.37
$4p4d\ ^3F_3$	3735.19	3773.27	3760.59		$4d4f\ ^3F_2$	7059.86	7100.89	7088.55
$4s4f\ ^3F_3$	4259.25	4272.82	4268.49		$4d4f\ ^1G_4$	7108.54	7140.84	7130.66
$4s4f\ ^3F_2$	4279.03	4300.18	4293.61		$4d4f\ ^3G_3$	7108.89	7152.09	7138.92
$4s4f\ ^3F_4$	4317.70	4327.00	4324.56		$4d4f\ ^3H_5$	7120.68	7154.15	7143.17
$4s4f\ ^3F_3$	4337.43	4354.47	4347.88		$4d4f\ ^3F_3$	7139.28	7186.51	7169.89
$4p4d\ ^3D_2$	4381.09	4397.20	4385.18		$4d4f\ ^3P_2$	7164.29	7209.02	7194.79
$4p4d\ ^3P_0$	4399.19	4418.65	4406.26		$4d4f\ ^3D_1$	7152.71	7213.14	7193.85
$4p4d\ ^3P_1$	4409.64	4429.33	4415.63		$4d4f\ ^3H_6$	7254.41	7278.68	7271.18
$4p4d\ ^3D_3$	4448.33	4476.17	4460.51		$4d4f\ ^3G_4$	7249.19	7279.97	7271.35
$4p4d\ ^3F_4$	4512.48	4518.51	4511.02		$4d4f\ ^3D_2$	7265.14	7304.52	7292.68
$4p4d\ ^3P_2$	4549.94	4558.66	4549.23		$4d4f\ ^3D_3$	7270.23	7314.49	7299.96
$4p4d\ ^1P_1$	4655.99	4683.67	4667.05		$4d4f\ ^3F_4$	7274.24	7308.93	7296.79
$4p4d\ ^1F_3$	4656.74	4692.27	4669.89		$4d4f\ ^3G_5$	7300.65	7344.09	7328.35
$4p4f\ ^3G_3$	5044.74	5084.54	5069.12		$4d4f\ ^3P_0$	7303.19	7352.99	7338.11
$4p4f\ ^3F_2$	5079.96	5127.11	5110.97		$4d4f\ ^3P_1$	7303.23	7352.02	7336.73
$4p4f\ ^3D_3$	5113.03	5149.19	5135.57		$4d4f\ ^3P_2$	7328.06	7368.19	7354.97
$4p4f\ ^3G_4$	5113.62	5149.98	5136.02		$4d4f\ ^1F_3$	7358.74	7402.50	7386.63
$4d^2\ ^3F_2$	5590.44	5639.55	5621.68		$4d4f\ ^1H_5$	7382.50	7441.60	7416.05
					$4d4f\ ^1P_1$	7412.09	7470.67	7449.52

results) coupling labels for each level. The LS labelling is taken from the COWAN code, while the jj labelling is from the HULLAC and RMBPT code. We already mentioned that in the recent compilation by Kramida and Shirai [56] only six energy values for two-electron states in W^{44+} were given, i.e. for E($3d^{10}4s4p\ ^{1,3}P_J$) and E($3d^{10}4s4d\ ^{1,3}D_2$). The best agreement (0.1%) between results given in the"COWAN" and "NIST" [56] columns of Table I is for the $3d^{10}4s4p\ ^1P_{01}$ level. Difference between the NIST [56] and RMBPT results of 0.02% -0.04% are obtained for the $3d^{10}4s4p\ ^{1,3}P_1$ and $3d^{10}4s4d\ ^{1,3}D_2$ levels.

Energies of the $3d^94l4l'4l$" core-excited states of Zn-like tungsten, obtained using COWAN and HULLAC codes are compared with the compilation of Kramida and Shirai [56] in Table II. The differences between the results from COWAN and HULLAC are given explicitly in Table II. Excellent agreement (0.1% - 0.4%) for the energies the $3d^94l4l'4l$" core-excited states is observed. This agreement is better than that was demonstrated in

TABLE II: Energies (10^3 cm^{-1}) of the $3d^9 4l4l'4l$" core-excited states of Zn-like tungsten, obtained using the COWAN and HULLAC codes. Our results are compared with compiled data from Kramida and Shirai [56]. Designations: $3d^9 4l4l'4l$" = $4l4l'4l$".

Conf	Level	Diff.	E (10^3 cm^{-1})			Conf	Level	Diff.	E (10^3 cm^{-1})		
		%	COWAN	HULLAC	[56]			%	COWAN	HULLAC	[56]
$4s^24p$	$(^2D)^3P_2$	0.1	13067.32	13054.14	13020	$4s4p^2$	$(^3P)^5P_1$	0.3	15180.56	15138.57	
$4s^24p$	$(^2D)^3F_3$	0.1	13074.50	13062.32	13020	$4s4p^2$	$(^1D)^3G_4$	0.2	15180.78	15157.70	
$4s^24p$	$(^2D)^3F_2$	0.2	13612.69	13583.96	13640	$4s^24d$	$(^2D)^3F_3$	0.2	15183.68	15155.57	
$4s^24p$	$(^2D)^3D_1$	0.2	13634.41	13612.08		$4s4p^2$	$(^1D)^3F_3$	0.1	15196.18	15182.49	
$4s4p^2$	$(^1S)^3D_3$	0.0	13823.13	13827.50		$4s4p^2$	$(^1D)^3D_2$	0.2	15197.92	15165.05	
$4s4p^2$	$(^3P)^3F^a{}_2$	0.0	13836.62	13841.61		$4s4p^2$	$(^1D)^3D_1$	0.2	15266.22	15237.99	
$4s^24p$	$(^2D)^3F_4$	0.3	13902.49	13859.76		$4s4p^2$	$(^1D)^3G_3$	0.2	15268.66	15242.82	
$4s^24p$	$(^2D)^1D_2$	0.3	13915.51	13876.88		$4s4p^2$	$(^1D)^3P_0$	0.2	15275.21	15245.75	
$4s^24p$	$(^2D)^1P_1$	0.3	13926.18	13888.46	13904	$4s4p^2$	$(^1D)^3F_2$	0.1	15287.70	15268.50	
$4s^24p$	$(^2D)^3D_3$	0.3	13935.86	13900.33		$4s4p^2$	$(^3P)^3F^b{}_2$	0.1	15298.71	15287.49	15280
$4s4p^2$	$(^3P)^5F_1$	0.1	14376.11	14366.03	14373	$4s^24d$	$(^2D)^1P_1$	0.2	15300.88	15271.03	
$4s4p^2$	$(^1S)^3D_2$	0.0	14385.83	14378.96	14390	$4s^24d$	$(^2D)^3G_5$	0.2	15302.47	15268.54	
$4s^24p$	$(^2D)^3P_0$	0.4	14425.50	14366.58		$4s4p^2$	$(^3P)^3P^b{}_1$	0.1	15307.43	15296.19	
$4s^24p$	$(^2D)^3P_1$	0.4	14456.26	14402.65		$4s^24d$	$(^2D)^3D_3$	0.2	15327.25	15298.69	
$4s^24p$	$(^2D)^3F_3$	0.4	14457.86	14403.28		$4s^24d$	$(^2D)^3F_4$	0.2	15331.43	15298.87	
$4s^24p$	$(^2D)^3D_2$	0.4	14475.21	14424.21		$4s^24d$	$(^2D)^1D_2$	0.2	15335.98	15310.67	
$4s4p^2$	$(^3P)^5D_4$	0.3	14555.11	14511.34		$4s4p^2$	$(^3P)^3P^b{}_0$	0.3	15421.69	15370.20	
$4s4p^2$	$(^3P)^5D_2$	0.3	14582.62	14544.31		$4s4p^2$	$(^3P)^5F_5$	0.3	15471.56	15426.82	
$4s4p^2$	$(^3P)^3D^a{}_1$	0.3	14590.18	14553.48	14568	$4s4p^2$	$(^1D)^3F_4$	0.2	15485.48	15450.92	
$4s4p^2$	$(^3P)^5P_3$	0.3	14590.27	14552.28		$4s4p^2$	$(^3P)^3P^a{}_1$	0.3	15492.80	15439.54	
$4s4p^2$	$(^1D)^3G_5$	0.2	14623.93	14593.64		$4s4p^2$	$(^1D)^3D_3$	0.3	15501.09	15460.05	
$4s4p^2$	$(^1D)^3P_2$	0.2	14644.26	14615.99	14626	$4s4p^2$	$(^1D)^3P_2$	0.3	15508.40	15465.24	
$4s4p^2$	$(^1D)^3D_3$	0.2	14644.39	14616.83		$4s^24d$	$(^2D)^3P_0$	0.1	15526.16	15507.08	
$4s4p^2$	$(^1D)^3F_4$	0.2	14648.02	14620.98		$4s4p^2$	$(^1S)^3D_3$	0.3	15584.13	15542.16	
$4s4p^2$	$(^1D)^1P_1$	0.2	14650.00	14621.94		$4s4p^2$	$(^1S)^1D_2$	0.2	15592.81	15555.49	
$4s4p^2$	$(^1D)^1S_0$	0.2	14657.10	14628.64		$4s4p^2$	$(^3P)^3F^b{}_4$	0.1	15612.64	15593.51	
$4s4p^2$	$(^1D)^3P_1$	0.1	14720.78	14702.45		$4s4p^2$	$(^3P)^3D^b{}_3$	0.2	15617.12	15590.20	
$4s4p^2$	$(^1D)^3G_4$	0.1	14726.02	14715.81		$4s4p^2$	$(^3P)^1P_1$	0.1	15625.18	15609.66	
$4s4p^2$	$(^3P)^3D^b{}_3$	0.1	14728.69	14720.79		$4s4p^2$	$(^3P)^3P^b{}_2$	0.1	15640.15	15618.52	
$4s4p^2$	$(^1D)^3D_2$	0.1	14735.78	14722.79	14715	$4s^24d$	$(^2D)^3G_3$	0.1	15704.75	15683.64	
$4s4p^2$	$(^3P)^1F_3$	0.0	14751.97	14755.33		$4s^24d$	$(^2D)^3D_1$	0.2	15704.99	15679.65	
$4s4p^2$	$(^3P)^3P^b{}_2$	0.0	14754.19	14756.02	14742	$4s4p4d$	$(^2D)^5P^a{}_1$	0.2	15727.07	15701.29	
$4s4p^2$	$(^3P)^5D_0$	0.4	15084.05	15023.48		$4s^24d$	$(^2D)^3F_2$	0.1	15739.43	15724.72	
$4s4p^2$	$(^3P)^5D_1$	0.4	15105.25	15048.07	15130	$4s4p4d$	$(^2D)^5D^a{}_2$	0.1	15756.00	15738.22	
$4s4p^2$	$(^3P)^5F_3$	0.3	15128.28	15075.60	15152	$4s4p4d$	$(^2D)^3H^a{}_4$	0.1	15764.82	15748.49	
$4s4p^2$	$(^3P)^5F_2$	0.4	15129.16	15075.54	15152	$4s4p4d$	$(^2D)^5F^b{}_3$	0.1	15776.40	15763.23	
$4s^24d$	$(^2D)^3P_1$	0.2	15139.45	15114.35		$4s4p4d$	$(^2D)^3P^a{}_0$	0.1	15801.68	15792.63	
$4s^24d$	$(^2D)^3G_4$	0.2	15163.19	15137.39		$4s4p4d$	$(^2D)^3D^b{}_1$	0.1	15809.91	15800.90	
$4s^24d$	$(^2D)^3D_2$	0.1	15172.22	15156.72		$4s4p4d$	$(^2D)^5H_5$	0.0	15813.64	15808.52	

Table I for two-electron excited states. The fourteen values of core-excited energies from Kramida and Shirai [56] are included in column [56] of Table II. A comparison of these values with the energies computed by the COWAN an HULLAC codes (columns "COWAN" and "HULLAC") confirms the accuracy of our calculations. The differences for the COWAN and HULLAC values is less than 0.4% and 0.5%, respectively.

In Table III, the wavelengths λ (in Å) and weighted radiative transition rates gA_r for transitions between the $3d^{10}4s^2\ {}^1S_0$ ground state and the $3d^{10}4s4p\ {}^{1,3}P_1$ excited states, as well as the $3d^9 4s4l4l'$ core-excited states in

TABLE III: Wavelengths (λ in Å) and weighted transition rates (A_r in s^{-1}) for transitions between the $3d^{10}4s^2\ ^1S_0$ ground state and the $3d^{10}4s4p\ ^{1,3}P_1$ excited states, as well as $3d^9 4s4ll'$ core-excited states in W^{44+} ion, obtained using the COWAN and HULLAC codes. Designations:: $3d^{10}4l4l' = 4l4l'$ and $3d^9 4l4l'4l" = 4l4l'4l"$. Numbers in brackets represent powers of 10.

Transitions		$\lambda_{\rm COWAN}$	$\lambda_{\rm HULLAC}$	$gA_r^{\rm COWAN}$	$gA_r^{\rm HULLAC}$
$4s4p$	$(^1S)^3P_1$	135.432	131.827	5.51[10]	7.23[10]
$4s4p$	$(^1S)^1P_1$	60.790	60.569	1.95[12]	2.56[12]
$4s^24p$	$(^2D)^3D_1$	7.329	7.346	1.58[13]	1.99[13]
$4s^24p$	$(^2D)^1P_1$	7.175	7.200	3.68[13]	3.45[13]
$4s^24p$	$(^2D)^3P_1$	6.911	6.943	5.39[12]	4.37[12]
$4s4p4d$	$(^2D)^3P_1^b$	6.231	6.235	1.87[12]	1.83[12]
$4s4p4d$	$(^2D)^5D_1$	6.173	6.174	6.00[11]	4.42[11]
$4s^24f$	$(^2D)^3P_1^d$	6.089	6.095	5.87[11]	7.70[11]
$4s4p4d$	$(^2D)^3P_1^g$	5.926	5.921	1.50[13]	1.16[13]
$4s4p4d$	$(^2D)^1P_1$	5.779	5.789	4.16[14]	3.54[14]
$4s4p4d$	$(^2D)^3D_1^f$	5.739	5.742	3.38[14]	3.50[14]
$4s4p4d$	$(^2D)^3D_1^h$	5.705	5.715	3.48[10]	4.09[10]
$4s4p4d$	$(^2D)^1P_1^f$	5.657	5.633	6.20[13]	7.43[13]
$4s4d4f$	$(^2D)^3D_1^j$	5.138	5.140	1.03[09]	7.58[08]
$4s4d4f$	$(^2D)^3P_1^d$	5.075	5.075	3.63[09]	5.24[09]
$4s4d4f$	$(^2D)^5P_1$	4.992	4.996	4.77[09]	5.53[09]
$4s4d4f$	$(^2D)^5F_1^d$	4.984	4.985	6.02[09]	5.51[09]
$4s4d4f$	$(^2D)^3D_1^h$	4.945	4.945	2.78[10]	2.98[10]
$4s4d4f$	$(^2D)^5P_1^b$	4.942	4.943	3.86[10]	2.77[10]
$4s4d4f$	$(^2D)^3D_1^b$	4.927	4.926	2.20[10]	2.71[10]
$4s^25p$	$(^2D)^1P_1$	4.784	4.792	1.01[13]	1.06[13]
$4s^25f$	$(^2D)^1P_1$	4.498	4.500	3.27[14]	4.01[14]
$4s^25f$	$(^2D)^1P_1$	4.397	4.401	3.97[14]	5.65[14]
$4s4d5p$	$(^2D)^3D_1^g$	4.226	4.229	2.67[10]	1.81[10]
$4s4d5p$	$(^2D)^1P_1^c$	4.191	4.194	1.83[10]	1.39[10]
$4s4d5p$	$(^2D)^5P_1^a$	4.175	4.179	9.81[08]	6.22[08]
$4s4d5p$	$(^2D)^3P_1^g$	4.105	4.112	4.69[08]	2.75[08]
$4s4d5p$	$(^2D)^3P_1^f$	4.092	4.096	2.33[10]	1.43[10]

W^{44+} ion obtained using COWAN and HULLAC are compared. The wavelength results are seen to agree with each other at the 0.1% to 0.5% level, while the radiative transition rates agree at the 10% to 50% level. The experimental wavelength value (60.931(2) Å) given in Ref. [62] for the $3d^{10}4s^2\ ^1S_0 - 3d^{10}4s4p\ ^1P_1$ transition is in better agreement with our COWAN value than with the HULLAC (compare second row in Table III, λ=60.79 Å and gA_r= 1.95[12] s^{-1}). The reverse is in the case of the $3d^{10}4s^2\ ^1S_0 - 3d^{10}4s4p\ ^3P_1$ transition. Its experimental value (132.88(3) Å) [63] is in better agreement with our HULLAC value (131.83 Å) than with our COWAN result.

III. DIELECTRONIC SATELLITE SPECTRA

The DR process to the bound states of the Zn-like ion occurs as an electron is captured by the Cu-like ion into an autoionizing state of the Zn-like ion followed by radiative decay to a singly excited bound state:

$$\begin{aligned} W^{45+}(3d^{10}4s) + e \ &\rightarrow\ W^{44+*}(3d^{10}4l_1nl + 3d^{10}5l_1nl + 3d^9 4l_1 4l_2 nl) \rightarrow W^{44+*}(3d^{10}4l_1'nl_2' + 3d^{10}5l_1'nl_2') + h\nu \\ &\downarrow \\ &\quad W^{45+}(3d^{10}4l) + e. \end{aligned} \tag{1}$$

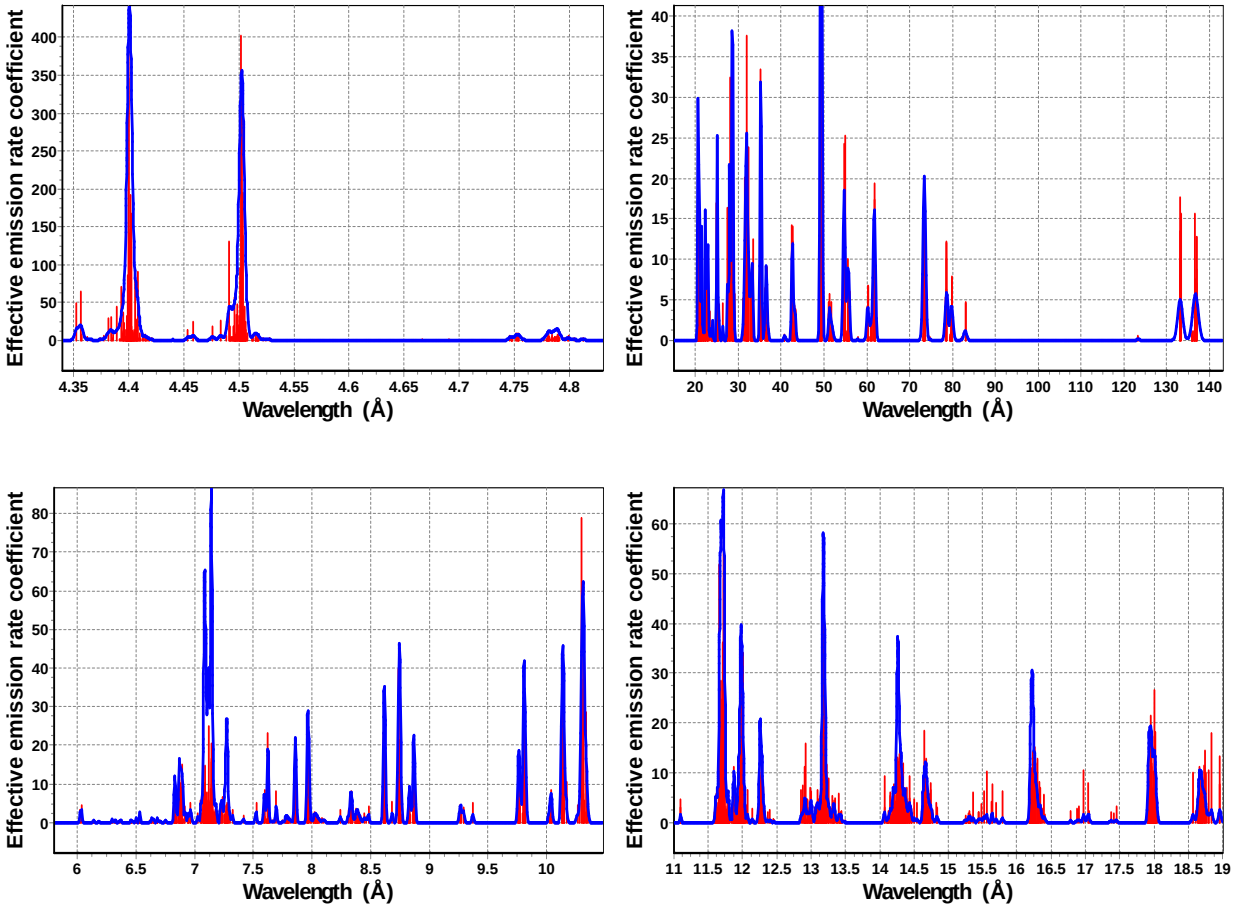

FIG. 1: (Color online) Synthetic spectra of dielectronic satellite lines (the $3d^{10}4l'nl - 3d^{10}4l_1nl_2$, $3d^{10}5l'5l - 3d^{10}5l_1nl_2$, and $3d^{10}4l'nl - 3d^{9}4l_14l_2nl$ transitions) from the W^{44+} ion at T_e = 800 eV for λ = 4.35 - 140 Å. A resolving power, $R = \lambda/\Delta\lambda$ = 1000, 100, and 500 in the top left, top right, and bottom panels, respectively is assumed to produce a Gaussian profile (thick line). The scale of the ordinate is in units of 10^{-15} cm^3/s.

The groundstate of W^{45+}, $3d^{10}4s$, is the initial state as we assume the plasmas are in coronal equilibrium. The autoionising states are divided into three type of states: the core-excited $3d^94l_14l_2nl_3$ states ($n_3 \geq 4$), the $3d^{10}4l_1nl_2$ states ($n_2 \geq 12$), and for $3d^{10}5l_1nl_2$ states ($n_2 \geq 8$). Among the core-excited $3d^94l_14l_2nl_3$ states, the $3d^94l_14l_25l_3$ states and $3d^94d^3$ are indeed autoionizing states, the $3d^94p^24d$ and $3d^94p4d^2$ are only partly autoionizing, and none of the doubly excited $3d^94s^24d$, $3d^94s^24d$, $3d^94s4p^2$, $3d^94s4d^2$, $3d^94s4p4d$, and $3d^94p^3$ configurations can autoionize. It is found that the two-electron $4l'nl$ ($n \geq 12$)states are all autoionizing except the $4s12l$ and $4p12p$ states. However, almost all $4dnl$ states are autoionizing already for $n \geq 9$. Some states ($4p12d$ and $4p9f$) are only partly autoionizing, The doubly excited $5l'nl$ ($n \geq 6$) are all autoionizing, however all $5l'5l$ states are non-autoionizing except the $5d^2$ states that only partly autoionizing.

During the DR process, dielectronic satellite lines are emitted when the electron jumps from doubly excited autoionization states to singly excited bound states. Radiative transitions from the $3d^{10}4pnl$ states to the $3d^{10}4snl$ states and those from the $3d^{10}5pnl$ states to the $3d^{10}4snl$ states give rise to satellite lines of the $4s-4p$ and $4s-5p$ lines of the Cu-like tungten. There also exist DR satellite transitions from autoionizing states $3d^{10}4dnl$ to $3d^{10}4pn'l$ with change of the principal quantum number n. They appear in a shorter wavelength region. Radiative transitions from the core-excited $3d^94l_14l_2n_4l_4$ to the excited non-autoionizing $3d^{10}4ln'l'$ states give rise to satellite lines to the $3d-nl$ (n =5, 6) transitions in Cu-like tungsten.

Branching ratios β and relative intensity factor Q_d of the dielectronic satellite (DS) lines are defined as (see,

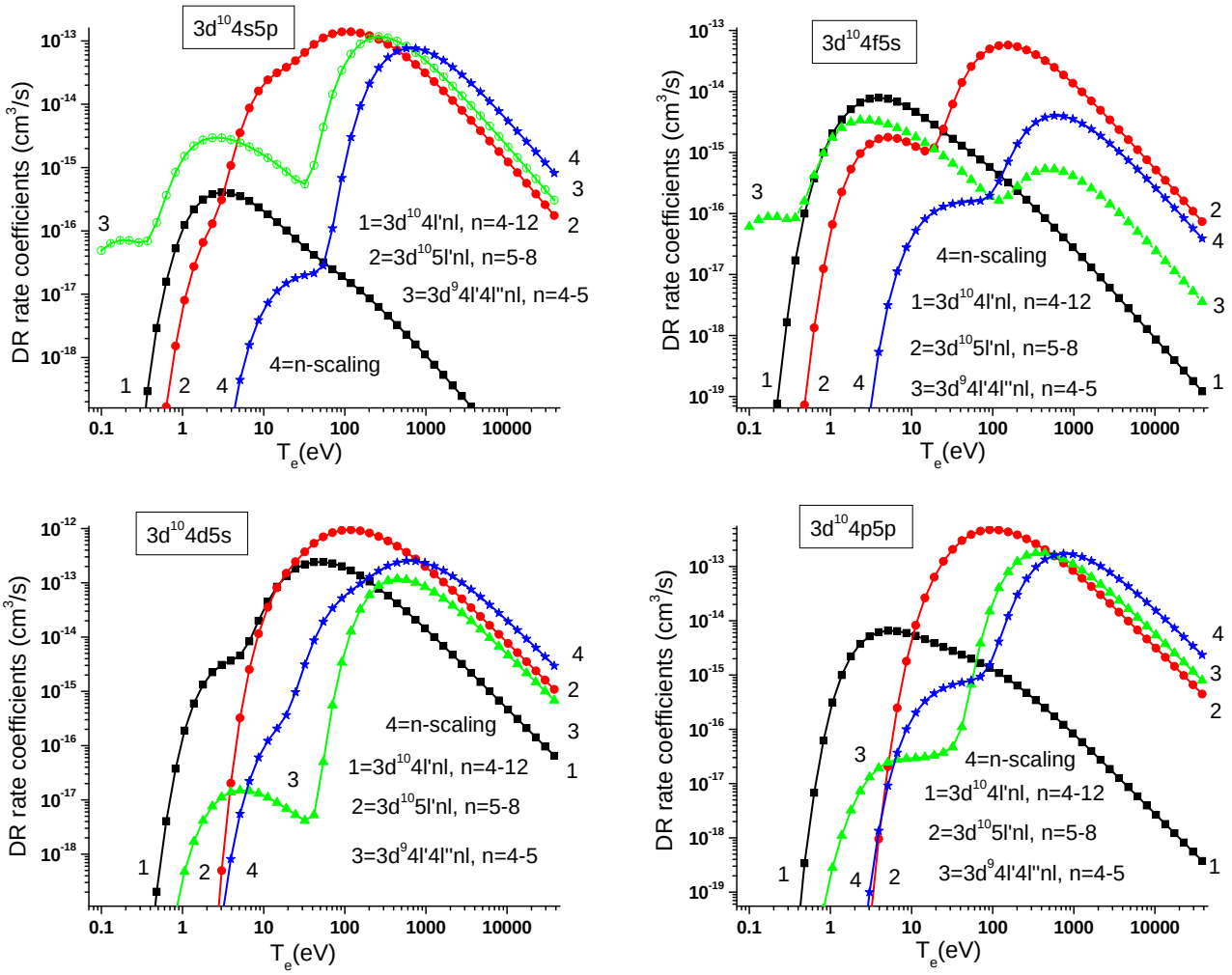

FIG. 2: (Color online) Contribution of the $3d^{10}4l'nl$, $3d^{10}5l'nl$ and $3d^{9}4l'4l''nl$ states to the DR rate coefficient $\alpha_d(3d^{10},j)$ for $j = 3d^{10}4s5p$, $3d^{10}4f5s$, $3d^{10}4d5s$, and $3d^{10}4p5p$ states as a function of T_e in Zn-like tungsten.

for example, Ref. [64])

$$\beta(i,i_0) = \frac{A_a(i,i_0)}{\sum_{i_0'} A_a(i,i_0') + \sum_k A_r(k,i)}, \qquad (2)$$
$$Q_d(j,i) = g(i)A_r(j,i)\beta(i,i_0)$$

Here j denotes the bound state, i is the autoionizing state, i_0 is the initial state (that is, the $3d^{10}4s$ ground state of the Cu-like ion), and i_0' is the possible final state for autoionization, e.g., $3d^{10}4s$. $g(i)$ is the statistical weight of the autoionizing state i, $A_a(i,i_0)$ is the autoionization rate from i to i_0, $A_r(j,i)$ is the radiative transition probability from i to j.

Assuming a Maxwellian distribution, the effective emission rate coefficient of dielectronic satellite line is obtained (see, for example, Ref. [65])

$$C_S^{\rm eff}(j,i) = 3.3\times10^{-24}\left(\frac{I_H}{kT_e}\right)^{3/2}\frac{Q_d(j,i)}{g_0} \qquad (3)$$
$$\times \exp\left(-\frac{E_S(i)}{kT_e}\right) \text{photons cm}^3\text{s}^{-1},$$

where I_H is the ionization potential of hydrogen, g_0 is the statistical weight of the initial state i_0, $E_S(i)$ is the excitation energy of the autoionizing state i relative to the $3d^{10}4s$ threshold, equal to 18990,000±11,000 cm^{-1}, or 2,354±1.4 eV [56], and T_e is the electron temperature. For cases where $A_a \gg A_r$ the branching ratio β (j,i) is about $\simeq$1, and the relative intensity factor Q_d is roughly estimated as $Q_d(j,i) \approx g(i)A_r(j,i)$. As already mentioned above, autoionization rates $A_a(i,i_0) = A_a(i,4s)$. We did not consider other channels for decay due to very cumbersome calculations. Results of our calculations of the effective emission rate coefficients $C_S^{eff}(j,i)$ are given in Tables IV, V, and VI.

Data for transitions between the $3d^{10}4l'nl$ excited and the $3d^{10}4l_1nl_1$ autoionization states, as well as between the $3d^{10}5l'5l$ excited and the $3d^{10}5l_1nl_1$ autoionization states are illustrated in Tables IV and V. It should be

TABLE IV: Autoionization rates (A_a in s^{-1}) and excitation energies (E_S in eV) of the $3d^{10}4l_1nl_2$ states as well as wavelengths (λ in Å), weighted radiative rates (gA_r in s^{-1}), intensity factors (Q_d in s^{-1}), and effective emission rate coefficients ($C_S^{\rm eff}$ in cm^3/s) for transitions between the $3d^{10}4l'nl$ excited and the $3d^{10}4l_1nl_2$ autoionization states of Zn-like tungsten. Designations: $3d^{10}4l'nl = 4l'nl$. The $C_S^{\rm eff}(j,i)$ values are given for $T_e = 800$ eV. The notation a[b] means a·10^b.

Level Lower	Level Upper	E_S eV	A_a s^{-1}	ΣA_a s^{-1}	ΣgA_r s^{-1}	gA_r s^{-1}	λ Å	Q_d s^{-1}	$C_S^{\rm eff}$ cm^3/s
				Even-odd-parity transitions					
$4d^2\ ^1G_4$	$4p12g\ ^1H_5$	7.0	1.46[13]	1.46[13]	2.42[13]	1.60[12]	7.524	1.39[12]	5.03[-15]
$4d^2\ ^3F_4$	$4p12g\ ^3G_5$	6.9	4.28[12]	4.28[12]	2.38[13]	2.18[12]	7.591	1.45[12]	5.26[-15]
$4p4f\ ^3G_5$	$4p12g\ ^3H_6$	7.1	1.09[13]	1.09[13]	2.85[13]	7.64[12]	7.624	6.36[12]	2.31[-14]
$4p5f\ ^1G_4$	$4p12g\ ^1H_5$	7.0	1.46[13]	1.46[13]	2.42[13]	3.52[12]	12.902	3.06[12]	1.11[-14]
$4d6g\ ^3I_7$	$4d9h\ ^3K_8$	27.6	6.65[12]	6.65[12]	3.22[13]	1.08[13]	28.699	8.38[12]	2.96[-14]
$4p10h\ ^3I_6$	$4d10h\ ^3K_7$	70.3	7.39[12]	7.39[12]	3.16[13]	1.32[13]	49.264	1.02[13]	3.43[-14]
$4p4f\ ^3G_5$	$4p12g\ ^3H_6$	7.1	1.09[13]	1.09[13]	2.85[13]	7.64[12]	7.624	6.36[12]	2.31[-14]
$4d5s\ ^3D_3$	$5s6f\ ^3F_4$	166.4	4.92[12]	4.92[12]	1.70[14]	6.00[13]	10.318	1.24[13]	3.69[-14]
$4f5d\ ^1H_5$	$5d6g\ ^1I_6$	366.7	8.57[12]	8.57[12]	2.36[14]	3.72[13]	11.662	1.19[13]	2.75[-14]
$4f5p\ ^3G_4$	$5p6g\ ^1H_5$	285.0	9.29[12]	9.29[12]	2.09[14]	6.18[13]	11.663	2.03[13]	5.19[-14]
$4s6g\ ^1G_4$	$5p6g\ ^1H_5$	285.0	9.29[12]	9.29[12]	2.09[14]	4.31[13]	11.705	1.41[13]	3.62[-14]
				Odd-even-parity transitions					
$4d5p\ ^3F_4$	$5p8f\ ^3G_5$	617.0	8.87[12]	8.87[12]	1.28[14]	3.04[13]	7.958	1.32[13]	2.23[-14]
$4d5p\ ^3F_4$	$5p7f\ ^3G_5$	478.2	1.02[13]	1.02[13]	1.49[14]	4.60[13]	8.736	1.98[13]	3.98[-14]
$4d5p\ ^3F_4$	$5p6f\ ^3G_5$	262.5	1.15[13]	1.15[13]	1.77[14]	7.18[13]	10.301	2.99[13]	7.88[-14]
$4s6f\ ^3F_4$	$5p6f\ ^3G_5$	262.5	1.15[13]	1.15[13]	1.77[14]	3.27[13]	11.711	1.36[13]	3.59[-14]
$4f5d\ ^3H_6$	$5d6g\ ^3I_7$	365.6	5.37[12]	5.37[12]	2.79[14]	1.18[14]	11.725	2.64[13]	6.11[-14]
$4p8g\ ^3H_5$	$5d8g\ ^3I_6$	696.3	5.81[12]	5.81[12]	1.57[14]	7.10[13]	11.974	2.30[13]	3.53[-14]
$4p6g\ ^3H_5$	$5d6g\ ^3I_6$	355.6	5.81[12]	5.81[12]	2.57[14]	6.38[13]	12.004	1.45[13]	3.40[-14]
$4p8g\ ^3H_6$	$5d8g\ ^3I_7$	706.8	4.07[12]	4.07[12]	1.59[14]	7.41[13]	13.173	2.05[13]	3.11[-14]
$4p7g\ ^1H_5$	$5d7g\ ^1I_6$	573.2	9.24[12]	9.24[12]	1.80[14]	5.76[13]	13.180	2.30[13]	4.12[-14]
$4p6s\ ^3P_2$	$5d6s\ ^3D_3$	205.5	4.41[12]	4.41[12]	9.65[13]	3.30[13]	13.197	8.00[12]	2.26[-14]
$4p6g\ ^3H_6$	$5d6g\ ^3I_7$	365.6	5.37[12]	5.37[12]	2.79[14]	7.01[13]	13.202	1.57[13]	3.64[-14]
$4d7f\ ^3H_6$	$5p7f\ ^3G_5$	478.2	1.02[13]	1.02[13]	1.49[14]	2.48[13]	17.951	1.07[13]	2.14[-14]
$4d6f\ ^3H_6$	$5p6f\ ^3G_5$	262.5	1.15[13]	1.15[13]	1.77[14]	2.42[13]	18.001	1.01[13]	2.65[-14]

noted that we do not need all 633,811 transitions to calculate the DR rate coefficients to excited states but rather only the transitions from the excited states (states under the first threshold $3d^{10}4s$) to the autoionizing states (states above the first threshold $3d^{10}4s$). The $3d^{10}4l_1nl$ states become autoionizing for $n_2 \geq 12$, the $3d^{10}5l_1nl$ states for $n_2 \geq 8$ and the $3d^{10}4snl$ states do not autoionize for any value of n. Thus, we obtain 142,272 transitions from the excited even-parity states to the autoionizing odd-parity states and 144,487 transitions from the excited odd-parity states to the autoionizing even-parity states. In Tables IV and V the transitions with the largest intensity factor Q_d are presented as an example.

Autoionization rates A_a and Auger energies E_S of the $3d^{10}4l_1nl_2$ and $3d^{10}5l_1nl_2$ states are listed in Tables IV and V, respectively. Transitions are divided among a set of even-odd-parity and odd-even-parity transitions. We present wavelengths, weighted radiative rates gA_r, intensity factors Q_d, and effective emission rate coefficients $C_S^{\rm eff}$ for the $3d^{10}4l'nl$ - $3d^{10}4l_1nl_2$ transitions in Table IV and for the $3d^{10}5l'nl$ - $3d^{10}5l_1nl_2$ transitions in Table V.

Most transitions given in Table IV are one-electron transitions such as $4p4f - 4p12g$, $4f5d - 5d6g$, $4d5p - 5p6f$, $4d8g - 5d8g$, $4d7f - 5p7f$. However, there are a few two-electron transitions (e.g., $4d^2 - 4p12g$) that appear due to configuration mixing (e.g. of $4d^2 + 4p4f$).

Among the $3d^{10}5l'nl$ - $3d^{10}5l_1nl_2$ transitions included in Table V, most transitions are one-electron transitions such as $5s5d - 5s8f$, $5s5g - 5s8h$, $5p5f - 5p6g$, $5p5d - 5p8f$, $5p5g - 5p8h$, and $5d5f - 5d7g$. However, there are a few two-electron transitions from states with equivalent electrons, as $5s^2$, $5p^2$, and $5d^2$. Transitions with the largest intensity factor Q_d in Table V are the transitions $5d^2 - 5p8g$, $5d^2 - 5p7g$, and $5p^2 - 5s6f$. These transitions are not zero due to the mixing between configurations, such as $[5d^2 + 5p5f]$ and $[5p^2 + 5s5d]$.

TABLE V: Autoionization rates (A_a in s^{-1}) and excitation energies (E_S in eV) of the $3d^{10}5l_1nl_2$ states as well as wavelengths (λ in Å), weighted radiative rates (gA_r in s^{-1}), intensity factors (Q_d in s^{-1}), and effective emission rate coefficients ($C_S^{\rm eff}$ in cm^3/s) for transitions between the $3d^{10}5l'5l$ excited and the $3d^{10}5l_1nl_2$ autoionization states of Zn-like tungsten. Designations: $3d^{10}5l'nl = 5l'nl$. The $C_S^{\rm eff}(j,i)$ values are given for $T_e = 800$ eV. The notation a[b] means a·10^b.

Level Lower	Level Upper	E_S eV	A_a s^{-1}	ΣA_a s^{-1}	ΣgA_r s^{-1}	gA_r s^{-1}	λ Å	Q_d s^{-1}	$C_S^{\rm eff}$ cm^3/s
				Even-odd-parity transitions					
$5s5d\ ^3D_3$	$5s8f\ ^3F_4$	521.0	3.52[12]	3.52[12]	1.30[14]	1.09[13]	15.636	2.14[12]	4.08[-15]
$5d^2\ ^1G_4$	$5p8g\ ^1H_5$	626.0	3.03[12]	3.03[12]	1.33[14]	5.64[12]	17.411	1.13[12]	1.89[-15]
$5s5g\ ^1G_4$	$5s8h\ ^1H_5$	532.9	3.03[12]	3.03[12]	1.40[14]	6.02[12]	18.006	1.16[12]	2.17[-15]
$5s5d\ ^3D_3$	$5s7f\ ^3F_4$	382.2	4.29[12]	4.29[12]	1.49[14]	1.63[13]	18.955	3.36[12]	7.62[-15]
$5d^2\ ^1G_4$	$5p7g\ ^1H_5$	491.9	5.03[12]	5.03[12]	1.61[14]	8.97[12]	21.451	2.29[12]	4.54[-15]
$5s^2\ ^1S_0$	$5s6p\ ^1P_1$	83.2	1.22[13]	1.22[13]	4.47[13]	2.44[12]	23.462	1.10[12]	3.62[-15]
$5p^2\ ^1D_2$	$5s6f\ ^1F_3$	165.0	1.09[13]	1.09[13]	1.26[14]	4.14[12]	26.329	1.56[12]	4.64[-15]
$5d^2\ ^1S_0$	$5d6f\ ^1P_1$	346.9	4.39[12]	4.39[12]	4.47[13]	4.42[12]	28.697	1.01[12]	2.38[-15]
$5p^2\ ^1D_2$	$5p6s\ ^1P_1$	125.0	9.08[12]	9.08[12]	4.43[13]	3.26[12]	28.773	1.24[12]	3.88[-15]
$5p5f\ ^3G_4$	$5p6g\ ^1H_5$	285.0	9.29[12]	9.29[12]	2.09[14]	2.40[13]	31.513	7.86[12]	2.01[-14]
$5p5f\ ^3G_4$	$5p6g\ ^3H_5$	235.0	4.68[12]	4.68[12]	1.99[14]	4.25[13]	32.480	8.73[12]	2.38[-14]
$5d^2\ ^3F_4$	$5p6g\ ^1H_5$	285.0	9.29[12]	9.29[12]	2.09[14]	7.03[12]	32.477	2.31[12]	5.91[-15]
$5p^2\ ^3P_2$	$5p6s\ ^1P_1$	125.0	9.08[12]	9.08[12]	4.43[13]	4.99[12]	32.737	1.90[12]	5.95[-15]
$5d^2\ ^1G_4$	$5p6g\ ^1H_5$	285.0	9.29[12]	9.29[12]	2.09[14]	1.49[13]	33.414	4.88[12]	1.25[-14]
				Odd-even-parity transitions					
$5p5d\ ^3F_4$	$5p8f\ ^3G_5$	617.0	8.87[12]	8.87[12]	1.28[14]	1.39[13]	15.560	6.02[12]	1.02[-14]
$5p5g\ ^3H_6$	$5p8h\ ^3I_7$	628.9	2.20[12]	2.20[12]	1.42[14]	1.49[13]	18.005	2.80[12]	4.67[-15]
$5p5g\ ^3H_5$	$5p8h\ ^3I_6$	579.3	1.51[12]	1.51[12]	1.13[14]	1.35[13]	18.033	2.00[12]	3.55[-15]
$5p5d\ ^3F_3$	$5p7f\ ^3G_4$	428.9	8.11[12]	8.11[12]	1.06[14]	1.51[13]	18.964	6.16[12]	1.32[-14]
$5d5f\ ^3H_5$	$5d7g\ ^3I_6$	562.3	6.26[12]	6.26[12]	1.99[14]	2.61[13]	20.885	7.56[12]	1.37[-14]
$5p5g\ ^3H_6$	$5p7h\ ^3I_7$	495.9	1.91[12]	1.91[12]	1.63[14]	3.24[13]	22.313	4.84[12]	9.53[-15]
$5p5d\ ^3F_2$	$5p6f\ ^3G_3$	211.4	8.19[12]	8.19[12]	1.09[14]	1.69[13]	27.463	5.81[12]	1.63[-14]
$5p5d\ ^3F_4$	$5p6f\ ^3G_5$	262.5	1.15[13]	1.15[13]	1.77[14]	2.96[13]	28.029	1.23[13]	3.25[-14]
$5d5f\ ^3H_6$	$5d6g\ ^3I_7$	365.6	5.37[12]	5.37[12]	2.79[14]	7.24[13]	31.863	1.62[13]	3.76[-14]
$5d5f\ ^3H_5$	$5d6g\ ^3I_6$	355.6	5.81[12]	5.81[12]	2.57[14]	4.82[13]	32.040	1.09[13]	2.57[-14]
$5p5g\ ^1H_5$	$5p6h\ ^1I_6$	291.7	3.97[11]	3.97[11]	1.71[14]	8.49[13]	35.287	2.49[12]	6.32[-15]
$5p5g\ ^3H_4$	$5p6h\ ^3I_5$	240.4	9.14[11]	9.14[11]	1.37[14]	7.51[13]	35.336	5.12[12]	1.39[-14]
$5p5g\ ^1F_3$	$5p6h\ ^1G_4$	293.4	6.76[11]	6.76[11]	1.21[14]	5.69[13]	35.428	2.72[12]	6.90[-15]

Autoionization rates and Auger energies for the core-excited the $3d^94l_14l_2nl$ states are illustrated in Table VI. It should be noted that the $3d^94l_14l_2nl$ core-excited states are not all autoionizing states. The $3d^94p^24d$ and $3d^94p4d^2$ configurations are only partly autoionizing. The energies of 205 levels of the $3d^94p^24d$ configuration are smaller than the threshold $3d^{10}4s$ energy, while 31 levels have a larger energy. An opposite split (54 and 332) of energies is found for the $3d^94p4d^2$ configuration. The energies of 192, 12, 38, 56, and 134 levels from the $3d^94s4p4d$, $3d^94s^24p$, $3d^94p^23$, $3d^94s4p^2$, and $3d^94s4d^2$ configurations, respectively, are smaller than the threshold $3d^{10}4s$ energy, and none of these levels can autoionize.

In Table VI, we illustrate our results for transitions between core-exited states. We consider the $3d^9(4s4p4d - 4p4d5p)$, $3d^9(4s4p4d - 4s4d5d)$, $3d^9(4s4p4d - 4s4d5s)$, $3d^9(4s4p4d - 4s4p5f)$, $3d^9(4s^24p - 4s4p5p)$, $3d^9(4s^24p - 4s^25d)$, $3d^9(4p^3 - 4p4d5p)$ and $3d^9(4p^3 - 4p^25d)$ transitions. These transitions are still one-electron ($4s - 5p$, $4p - 5s$, $4p - 5d$, and $4d - 5f$) transitions; an exception is the two-electron $3d^9(4p^3 - 4p4d5p)$ transition. It should be noted that the values of E_S, A_a, A_r, Q_d, and $C_S^{\rm eff}$ for transitions between core-excited states and transitions between the excited and core-excited states also listed in Table VI are of similar order of magnitude. The difference is only in wavelength: about 11 Å and about 5 Å. Most of the $3d^{10}4l'nl$ - $3d^94l_14l_2nl$ transitions given in Table VI are also one-electron $3d - 5f$, $3d - 5p$, and $3d - 4p$ transitions. Using the short designations from Table VI, we find these to be the $4p^2 - 4p^25f$, $4s4d - 4s4d5f$, $4s4p - 4s4p5f$, $4s4d - 4s4d5p$, $4s5p - 4s4p5p$, and $4p4d - 4p^24d$ transitions.

TABLE VI: Autoionization rates (A_a in s^{-1}) and excitation energies (E_S in eV) of the $3d^{10}4l_1nl_1$ states as well as wavelengths (λ in Å), weighted radiative rates (gA_r in s^{-1}), intensity factors (Q_d in s^{-1}), and effective emission rate coefficients ($C_S^{\rm eff}$ in cm^3/s) for transitions between $3d^{10}4l'nl$ excited and $3d^94l_14l_2nl$ doubly excited autoionization states of Zn-like tungsten. Transitions between doubly excited non-autoionization and autoionization states are included. Designations: $3d^{10}nl'nl = nl'nl$ and $3d^94l_14l_2nl = 4l_14l_2nl$. The $C_S^{\rm eff}(j,i)$ values are given for T_e = 800 eV. The notation a[b] means a·10^b.

Level Lower	Level Upper	E_S eV	A_a s^{-1}	ΣA_a s^{-1}	ΣgA_r s^{-1}	gA_r s^{-1}	λ Å	Q_d s^{-1}	$C_S^{\rm eff}$ cm^3/s
				Even-odd-parity transitions					
$4s^2\ ^1S_0$	$4s4p5d\ ^3P_1$	473.3	3.90[13]	3.90[13]	3.45[13]	1.91[13]	4.385	1.48[13]	2.99[-14]
$4p^2\ ^3P_2$	$4p^25f\ ^3D_3^e$	866.4	4.49[12]	4.49[12]	7.22[14]	7.14[14]	4.396	2.98[13]	3.69[-14]
$4s4d\ ^3D_2$	$4s4d5f\ ^3D_2^f$	808.9	3.63[11]	3.63[11]	5.70[12]	4.39[14]	4.401	1.06[14]	1.41[-13]
$4s4d\ ^3D_2$	$4s4d5f\ ^3F_3^n$	808.7	3.15[13]	3.15[13]	4.24[14]	4.23[14]	4.402	1.45[14]	1.92[-13]
$4s4d\ ^3D_1$	$4s4d5f\ ^5F_2^d$	805.5	1.82[11]	1.82[11]	6.87[10]	1.18[14]	4.402	1.10[14]	1.47[-13]
$4s4d\ ^3D_3$	$4s4d5f\ ^1F_3^j$	826.6	2.95[11]	2.95[11]	9.44[11]	1.87[14]	4.403	1.28[14]	1.67[-13]
$4p^2\ ^3P_2$	$4p^25f\ ^1F_3$	805.7	5.32[10]	5.32[10]	3.22[12]	1.28[14]	4.492	1.33[13]	1.77[-14]
$4p^2\ ^3P_2$	$4s4d5f\ ^3F_2$	804.0	4.38[12]	4.38[12]	8.40[13]	6.48[13]	4.495	1.34[13]	1.79[-14]
				Odd-even-parity transitions					
$4s4p\ ^1P_1$	$4p^25d\ ^3F_2^c$	670.8	1.53[12]	1.53[12]	7.19[13]	5.56[13]	4.394	5.36[12]	8.47[-15]
$4s4p\ ^1P_1$	$4s4p5f\ ^3D_2^e$	668.4	2.24[12]	2.24[12]	1.08[14]	9.61[13]	4.398	8.99[12]	1.43[-14]
$4s4p\ ^3P_1$	$4s^25d\ ^3P_0$	320.0	2.63[13]	2.63[13]	6.86[12]	2.76[12]	4.800	2.19[12]	5.37[-15]
$4p4d\ ^3P_2$	$4p4d5p\ ^3D_3^f$	822.5	1.25[12]	1.25[12]	2.07[13]	1.45[13]	4.746	4.31[12]	5.64[-15]
$4p4d\ ^3F_4$	$4p24d\ ^5P_3^a$	3.5	1.08[13]	1.08[13]	7.55[12]	4.50[12]	6.895	4.09[12]	1.49[-14]
$4s5f\ ^1F_3$	$4s4p5f\ ^1G_4^a$	663.2	2.86[12]	2.86[12]	4.93[13]	4.77[12]	6.822	1.64[12]	2.61[-15]
$4p5d\ ^3P_2$	$4p^25d\ ^5D_3^a$	786.9	4.02[12]	4.02[12]	7.73[12]	1.71[12]	6.828	1.34[12]	1.83[-15]
$4d5p\ ^3D_1$	$4p4d5p\ ^3F_2^r$	802.0	9.80[11]	9.80[11]	1.90[13]	5.62[12]	6.845	1.15[12]	1.55[-15]
$4s5p\ ^3P_2$	$4s4p5p\ ^3D_3^d$	441.1	4.61[11]	4.61[11]	4.22[13]	2.87[13]	7.076	2.04[12]	4.29[-15]
$4p5s\ ^3P_2$	$4p^25s\ ^3D_3$	545.3	2.78[11]	2.78[11]	3.59[13]	2.80[13]	7.083	1.44[12]	2.66[-15]
$4p5s\ ^3P_2$	$4s4p5f\ ^5H_3^a$	545.2	1.08[12]	1.08[12]	4.06[13]	2.75[13]	7.083	4.32[12]	7.99[-15]
				Transitions between core-excited states					
$4s4p4d\ ^3D_1^c$	$4p4d5p\ ^3P_2^l$	694.9	3.11[12]	3.11[12]	1.12[13]	6.51[12]	11.618	3.78[12]	5.80[-15]
$4s4p4d\ ^3F_2^b$	$4s4d5d\ ^3D_2^n$	672.3	1.50[13]	1.50[13]	1.49[13]	1.63[12]	11.641	1.36[12]	2.15[-15]
$4s4p4d\ ^3P_0$	$4s4d5s\ ^3S_1^b$	586.5	1.11[14]	1.11[14]	1.58[13]	3.15[12]	14.149	3.01[12]	5.28[-15]
$4s4p4d\ ^5H_3$	$4s4p5f\ ^5I_4$	538.6	6.11[11]	6.11[11]	1.13[14]	8.79[13]	14.206	4.10[12]	7.64[-15]
$4s^24p\ ^3D_1$	$4s4p5p\ ^5P_1^b$	393.2	2.11[12]	2.11[12]	2.53[13]	5.31[12]	11.727	1.06[12]	2.38[-15]
$4s^24p\ ^3D_1$	$4s4p5p\ ^5D_0$	384.0	1.28[13]	1.28[13]	5.61[12]	1.81[12]	11.830	1.26[12]	2.85[-15]
$4s^24p\ ^3P_2$	$4s^25d\ ^3P_1$	303.1	7.60[11]	7.60[11]	1.73[13]	1.45[13]	11.951	1.68[12]	4.21[-15]
$4p^3\ ^5D_1$	$4p4d5p\ ^3D_2^h$	698.3	4.01[12]	4.01[12]	9.02[12]	1.69[12]	11.657	1.17[12]	1.78[-15]
$4p^3\ ^1S_0$	$4p^25d\ ^1P_1^a$	707.3	1.84[12]	1.84[12]	2.31[13]	7.63[12]	11.957	1.47[12]	2.22[-15]

Figure 1 shows examples of dielectronic satellite spectra with kT_e=800 eV for the $3d^{10}4l'nl - 3d^{10}4l_1nl_2$, $3d^{10}5l'5l - 3d^{10}5l_1nl_2$, and $3d^{10}4l'nl - 3d^94l_14l_2nl$ transitions. In the four panels of Fig. 1, we include data for 1965 even-odd-even parity transitions. The effective emission rate coefficients $C_S^{eff}(j,i)$ and Gaussian profiles with spectral resolution $R \equiv \lambda/\Delta\lambda = 1000$ (top left panel), 100 (top right panel), and 500 (bottom panels) are used to synthesize these spectra (see for detail, for example, Ref. [66]). The limited set of transitions includes transitions with $C_S^{eff}(j,i) > 10^{-16}$ cm^3/s. The synthetic spectrum of dielectronic satellite lines from the W^{44+} ion at $T_e = 800$ keV is divided into four parts: $\lambda = 4.35$ Å to 4.85 Å , $\lambda = 6$ Å to 11 Å , λ =11 Å to 19 Å , and λ = 20 Å to 140 Å. Below, in this section, we use the short designations nl instead of $3d^{10}nl$, $4l'nl$ instead of $3d^{10}4lnl$, $5l'nl$ instead of $3d^{10}5l'nl$, and $4l4l'nl_1$ instead of $3d^94l4l'nl_1$.

The intensity of lines shown on the top left panel of Fig. 1 is larger by a factor of 5-10 than all other lines shown on the three other panels of Fig. 1. Eleven lines with $C_S^{\rm eff}$ equal to 141–392×10^{-15} cm^3/s are due to the $4s4d - 4s4d5f$ transitions. Of these six lines are distributed in a very small interval from $\lambda = 4.4001$ Å up to $\lambda = 4.4026$ Å . The remaining five lines are distributed

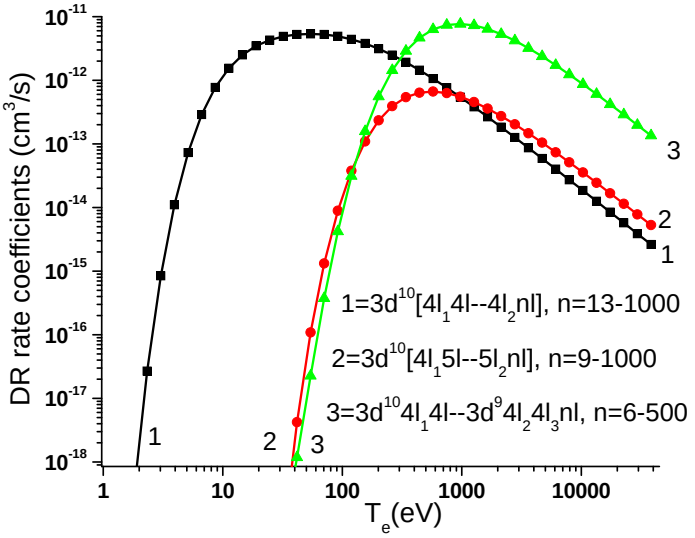

FIG. 3: (Color online) Sum of the $3d^{10}[4l_14l-4l_2nl]$ with n = 13-1000, $3d^{10}[4l_15l-5l_2nl]$ with n = 9-1000, and $3d^{10}4l_14l-3d^94l_24l_3nl$ with n = 6-500 contributions to the total DR rate coefficient $\alpha_d(3d^{10}4s)$ as a function of T_e in Zn-like tungsten.

in a 0.0125 Å wide interval from λ = 4.4913 Å up to λ = 4.5038 Å . The values of A_a, E_S, gA_r, Q_d, and $C_S^{\rm eff}$ for four of these lines are shown by lines 3-6 in Table VI.

The strongest lines shown on the top right panel of Fig. 1 are due to the Rydberg transitions ($4p9h-4d9h$, $4p9h-4d9h$, $4p12h-4d12h$, $4p11h-4d11h$, $4p10h-4d10h$) distributed in a small interval from λ = 49.23 Å up to λ = 49.26 Å . The $C_S^{\rm eff}$ values are equal to 21–34$\times10^{-15}$ cm^3/s. Similarly strongest lines are found in the region of 28 Å to 32 Å, they are due to the even-odd parity $5p5f-5p6g$ transitions as well as the odd-even parity $5p5d-5p6f$ and $5d5f-5d6g$ transitions. The values of A_a, E_S, gA_r, Q_d, and $C_S^{\rm eff}$ for these five lines are shown in Table V.

A large number of satellite lines to the $4d-nf$ transitions ($4d5p-5pnf$ with n = 8, 7, 6) are responsible for the spectral features shown in the bottom left panel of Fig. 1 in the very narrow region of λ = 8.61 - 8.75 Å and λ = 10.14 - 10.34 Å. The strong contributions from the $4f5d-5d7g$ transition fall into the very small region λ = 9.76 - 9.82 Å. The values of A_a, E_S, gA_r, Q_d, and $C_S^{\rm eff}$ for some of these lines are given in the odd-parity part of Table IV. A number of satellite lines to the $3d-4p$ transitions ($4p4d-4p^24d$, $4d5p-4p4d5p$, $4s5f-4s4p5f$, $4s5d-4s4d5d$, $4p5f-4p^25f$) are responsible for the spectral features shown at λ = 6.86- 7.14 Å in the bottom left panel Fig. 1.

The intensity of the lines shown on the bottom right and left panels of Fig. 1 are almost the same, about 0–80$\times10^{-15}$ cm^3/s. Both spectra are formed by transitions illustrated in Table IV. The $4s-5p$ ($4s6f-5p6f$, $4s7f-5p7f$, $4s8f-5p8f$, $4s6g-5p6g$) and $4f-6g$ ($4f5d-5d6g$) transitions form features in the narrow region of 11.66 - 11.74 Å. Another feature in the narrow region 11.97 - 12.00 Å is formed by $4p-5d$ ($4p8g-5d8g$, $4p7g-5d7g$, $4p6g-5d6g$) transitions. Lines in the narrow region 13.17-13.20 Å have intensity 20–40$\times10^{-15}$ cm^3/s. The lines in this interval are due $4p8g-5d8g$, $4p7g-5d7g$, $4p6g-5d6g$, $4p6s-5d6s$, $4p7i-5d7i$ transitions. The intensity of lines in the interval 14-19 Å shown on the bottom right panel of Fig. 1 is less than 10-15$\times10^{-15}$ cm^3/s.

IV. DIELECTRONIC RECOMBINATION RATE COEFFICIENTS FOR EXCITED STATES

The DR rate coefficients for excited states are obtained by the summation of the effective emission rate coefficients $C_S^{eff}(j,i)$ (Eq. (3)) for DR processes through all possible intermediate doubly excited states:

$$\alpha_d(i_0,j)=\sum_i C_S^{eff}(j,i). \qquad (4)$$

Ḟor the DR process described by Eq. (4), one has to calculate $\alpha_d(i_0,j)$ with $i_0=3d^{10}4s$ and all possible excited states j of W^{44+} with energies below the first threshold, $3d^{10}4s$ (18,990,000 cm^{-1}). Below, we present our results without LSJ. This means that we sum our numerical results over all LSJ values to reduce the very large number of levels for presentation. We evaluate energies and radiative and non-radiative transitions for the $3d^{10}4l'nl$ states with n =4-12 and $l'=s,p,d,f,g,h,i,k$. Among these states, the energies of the $3d^{10}4snl$ states with n =4-12 and l' = 0 -7 are lower than 18,990,000 cm^{-1}. It is found that the energies of the $3d^{10}4pnl$ states with n =4-12 and $l=s,p,d$ are below the threshold, while with the $l=f,g,h,i,k$ are above threshold. The energies of $3d^{10}4dnl$ states with n =4-9 and $l=s,p,d$ are below threshold, while those with $l=f,g,h,i,k$ are above the threshold. All together 819 levels of odd parity and 814 levels of even parity for the $3d^{10}4l'nl$ configurations have energies lower than 18,990,000 cm^{-1}.

Among the $3d^{10}5l'5l$ states, there are also 35 even-parity states ($3d^{10}5s^2$, $3d^{10}5p^2$, $3d^{10}5d^2$, $3d^{10}5s5d$ and $3d^{10}5p5f$) and 52 odd-parity states ($3d^{10}5s5p$, $3d^{10}5s5f$, $3d^{10}5p5d$, $3d^{10}5p5g$, and $3d^{10}5d5f$) with energies lower than 18,990,000 cm^{-1}. The core-excited $3d^94l_14l_24l_3$ configurations also contributes to non-autoionizing states. There are 413 even-parity states ($3d^94s4p^2$, $3d^94s4d^2$, $3d^94s^24d$, and $3d^94p^24d$) and 293 odd-parity states ($3d^94s^24p$, $3d^94s4p4d$, $3d^94p4d^2$, and $3d^94p^3$) with energies lower than 18,990,000 cm^{-1}.

The sum over i includes the $3d^{10}4l'nl$ autoionizing states with energies larger than 18,990,000 cm^{-1}, i.e., 260 even-parity levels and 296 odd-parity levels. For the $3d^{10}5l'nl$ states the index i is equal to 308 and 324 for even-parity and odd-parity states, respectively. The number of core-excited $3d^94l'4l''nl$ autoionizing states is equal to 1768 and 2142 for even-parity and odd-parity states, respectively.

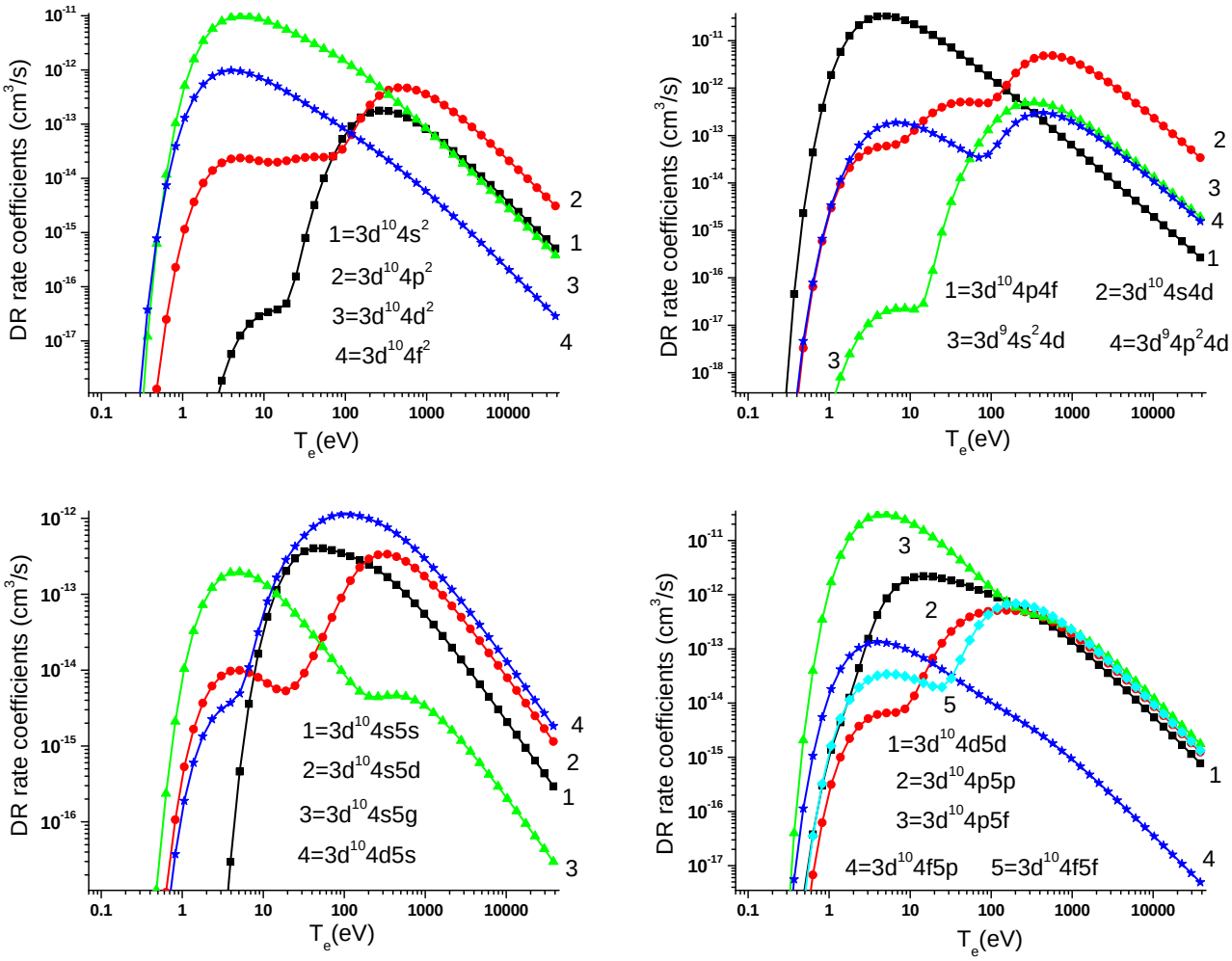

FIG. 4: (Color online) Dielectronic Recombination rate coefficient $\alpha_d(3d^{10}, j)$ for $j = 3d^{10}4l^2$, $3d^{10}4p4f$, $3d^{10}4s4d$, $3d^{10}4s5l_1$, $3d^{10}4d5l_1$, $3d^{10}4p5l_2$, $3d^{10}4f5l_2$ ($l_1 = s, d, g$ and $l_2 = p, f$), $3d^94s^24d$, and $3d^94p^24d$ states as function of T_e in Zn-like W.

In Fig. 2, we illustrate the contributions to the DR rate coefficient $\alpha_d(3d^{10}4s, j)$ for a subset of states including $j = 3d^{10}4s5p$, $3d^{10}4f5s$, $3d^{10}4d5s$, and $3d^{10}4p5p$ states. The sum over i includes states with n = 4-12 (for $4l'nl$ autoionizing states), n = 5-8 (for $5l'nl'$ autoionizing states), and n = 4-5, (for $3d^94l'4l''nl$ core-excited states). Those contributions are represented by curves 1, 2, and 3 curves, respectively. In Fig. 2, we show $\alpha_d(3d^{10}4s, j)$ with $j = 3d^{10}4s5p$, $3d^{10}4f5s$, $3d^{10}4d5s$, and $3d^{10}4p5p$ states. It was already mentioned that we sum our results over LSJ. For example, the $\alpha_d(3d^{10}4s, 3d^{10}4s5p)$ values include results for four levels: $\alpha_d(3d^{10}4s, 3d^{10}4s5p\ ^3P_0)$ + $\alpha_d(3d^{10}4s, 3d^{10}4s5p\ ^3P_1)$ + $\alpha_d(3d^{10}4s, 3d^{10}4s5p\ ^3P_2)$ + $\alpha_d(3d^{10}4s, 3d^{10}4s5p\ ^1P_1)$.

One can see that curve 2 is above curve 1 for the $3d^{10}4s5p$ states for the entire interval of T_e, while curve 2 is under curve 1 for low temperatures in three other states illustrated in Fig. 2. That means that the contribution of the $3d^{10}4l'nl$ autoionizing states is more important at low temperatures (1 eV to 5 eV) than the contribution of the $3d^{10}4lnl'$ autoionizing states, while at higher temperatures their relative contributions are opposite. The contributions of the $3d^94l'4l''nl$ states (curve 3) are more important for very high temperature T_e (larger than 1000 eV). However, the curve is above all curves in the top two panels for very small T_e (near threshold). It is clearly seen that the contributions of the $3d^{10}4l'nl$, $3d^{10}5l'nl$, and $3d^94l'4l''nl$ states in the sum over i in Eq. (4) change with temperature, and all three types of states are important for the calculation of $\alpha_d(3s, j)$ for different values of j.

Below, in this section, use the short designations nl instead of $3d^{10}nl$, $4l'nl$ instead of $3d^{10}4l'nl$, $5l'nl$ instead of $3d^{10}5l'nl$, and $3d4l'4l''nl$ instead of $3d^94l'4l''nl$.

In order to estimate the contributions from the high-n autoionizing states to the DR rate coefficients for excited states (sum over i with $n > 12$ for autoionizing $4l'nl$ states, sum over i with $n > 8$ for autoionizing $5l'nl$ states, and sum over i with $n > 5$ for core-excited $3d4l'4l''nl$ states), we use empirical scaling laws [67], which can

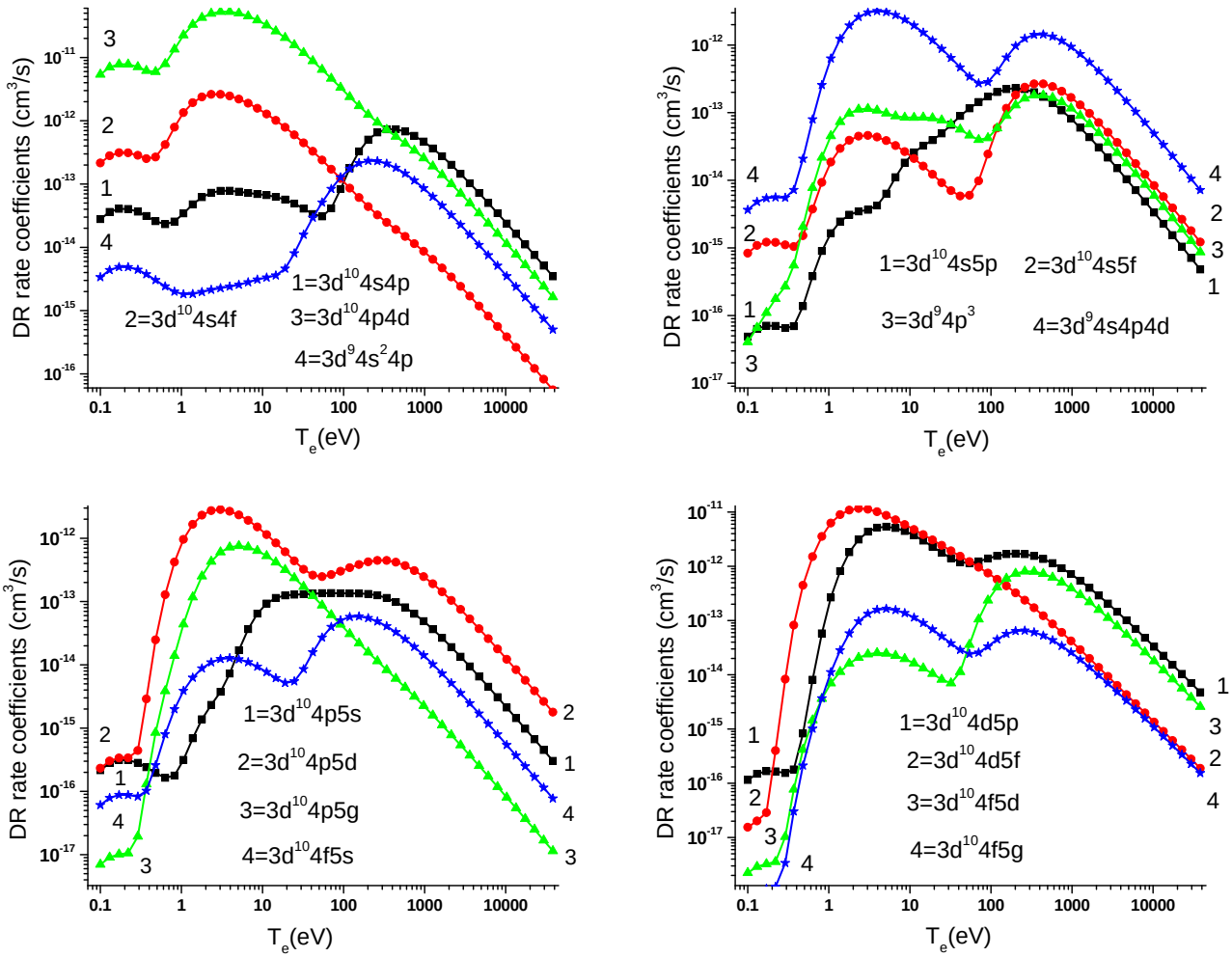

FIG. 5: (Color online) Dielectronic Recombination rate coefficient $\alpha_d(3d^{10}, j)$ for $j = 3d^{10}4s4p$, $3d^{10}4s4f$, $3d^{10}4p4d$, $3d^{10}4s5l_1$, $3d^{10}4d5l_1$, $3d^{10}4p5l_2$, $3d^{10}4f5l_2$ ($l_1 = p, f$ and $2_1 = s, d, g$), $3d^9 4s^2 4p$, $3d^9 4p^3$, and $3d^9 4s4p4d$ states as function of T_e in Zn-like W.

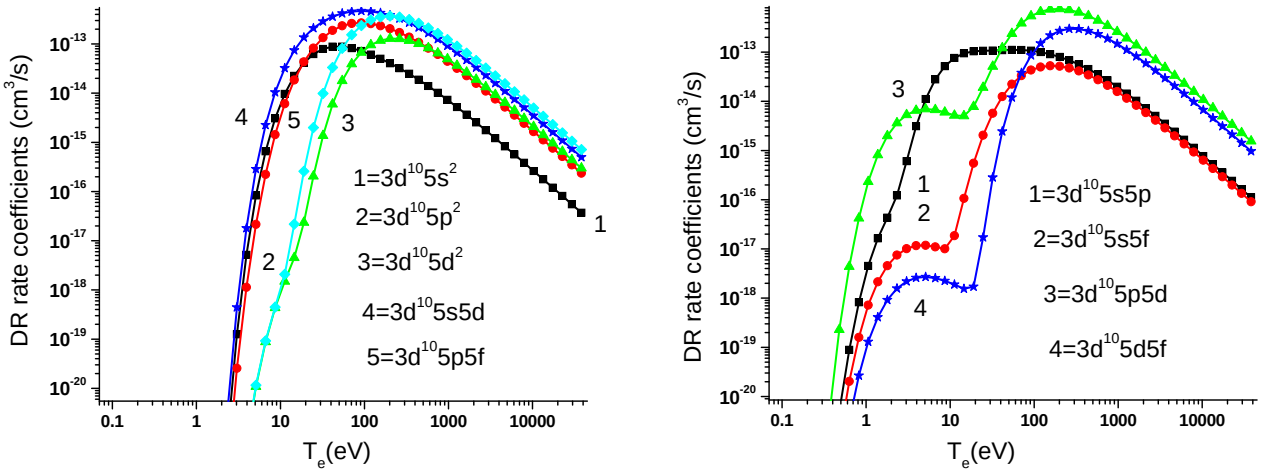

FIG. 6: (Color online) Dielectronic Recombination rate coefficient $\alpha_d(3d^{10}, j)$ for $j = 3d^{10}5l^2$ ($l = s, p, d$), $3d^{10}5s5d$, $3d^{10}5p5f$, $3d^{10}5s5p$, $3d^{10}5s5f$, $3d^{10}5p5d$, and $3d^{10}5d5f$ states as function of T_e in Zn-like W.

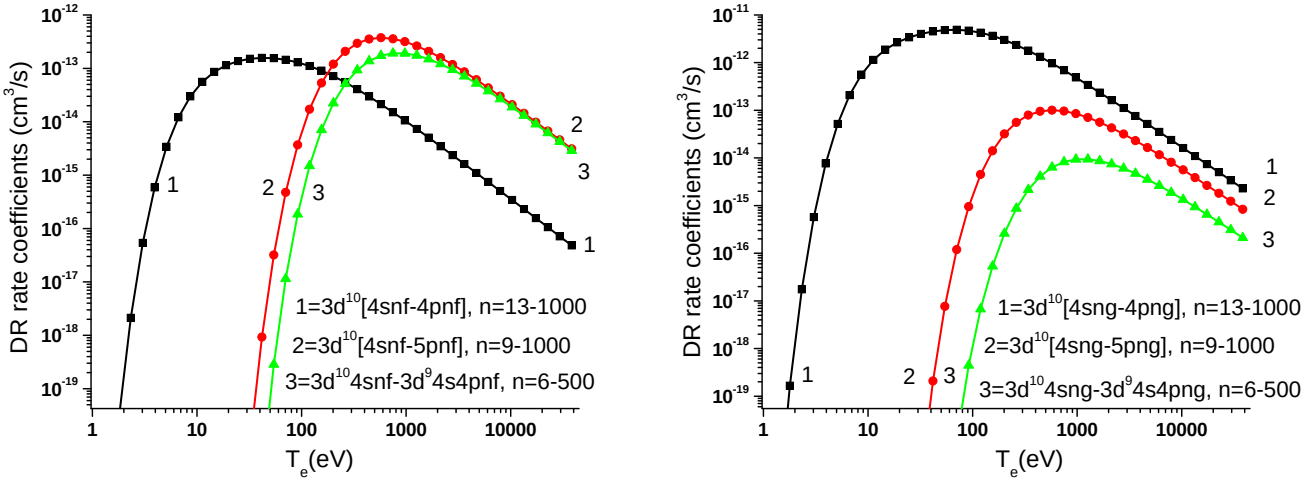

FIG. 7: (Color online) The $3d^{10}[4snl-4pnl]$, $3d^{10}[4snl-5pnl]$, and $3d^{10}4snl-3d^94s4pnl$ ($l=f,g$) contributions to the total DR rate coefficient $\alpha_d(3d^{10}4s)$ resulting from summation over i and j in Eq. (5).

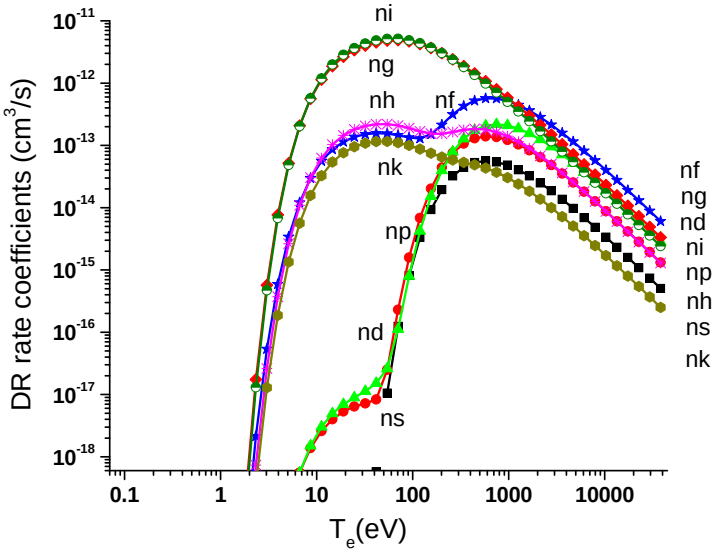

FIG. 8: (Color online) Sum of the $3d^{10}[4sn_1l-4pn_1l]$, $3d^{10}[4sn_2l-5pn_2l]$, and $3d^{10}4sn_3l-3d^94s4pn_3l$ ($l=s,p,d,f,g,h,i,k$, n_1 = 13-1000, n_2 = 9-1000, and n_3 = 6-500) contributions to the total DR rate coefficient $\alpha_d(3s)$ as a function of l and T$_e$ in Zn-like tungsten.

only be implemented to include the one-electron $4s-np$, $4p-ns$, $4p-nd$, $4d-np$, $4d-nf$, $3d-np$, and $3d-nf$ dipole transitions. Additional contributions from the high-n states appear for the first low-lying configurations $4l4l'$ and $4l5l'$. For these configurations the $[4s4p-4pnp]$, $[4s4d-4dnp]$, $[4p4d-4pnp,4pnf,4dns,4dnd]$, $[4p^2-4pns,4pnd]$, and $[4d^2-4dnp,4dnf]$ transitions with $n>13$ are to be included as well. Transitions with $n>8$ are taken into account for the $4l4l'$ configurations: $[4s5s-5snp]$, $[4s5p-5pnp]$, $[4s5f-5fnp]$, $[4p5s-5sns,5snd]$, $[4p5p-5pns,5pnd]$, $[4p5d-5dns,5dnd]$, $[4p5f-5fns,5fnd]$, $[4d5s-5snp,5snf]$, $[4d5p-5pnp,5pnf]$, $[4d5d-5dnp,5dnf]$, and $[4d5f-5fnp,5fnf]$. Transitions with $n>5$ core-excited states are taken into account for the $4l4l'$ configurations: $[4s4l'-3d4s4l'np]$ and $4s4l'-3d4s4l'nf]$. Scaling contributions for the $4l5l'$ configurations from the core-excited $3d4l'4l''nl$ states with $n>5$ are due to the mixing of the $[4l4l'+4l5l']$ configurations.

To estimate $Q_d(j,i)$ in Eq.(3) for autoionizing states i with high principal quantum number n for the $4l5l'$ states (for example, for the $4s5s-5snp$ dipole transitions) we used the calculated data for $n=8$ and the $1/n^3$ scaling law for A_a and A_r (see for detail Ref. [19]).

The results of the calculations are shown in Fig. 2. In order to test the scaling, we compared the explicitly calculated data for $n=12$ and the scaled data for $n=12$ derived from the calculated data for $n=11$. We found that the difference is within 10 % except for some cases when the mixing of configurations is very important. The contributions from the scaled data are shown by curve 4 in four panels of Fig. 2. The values represented by this curve includes the scaled data from $n=13$ up to $n=1000$ of the $4lnl'$ autoionizing states, from $n=9$ up to $n=500$ of the $5lnl'$ states, and from $n=5$ up to $n=100$ of the $3d4l'4l''nl$ core-excited states. The reason why we change the n for the explicitly and scaled data sets is that the sum involves more states. For example,we sum over 190, 357, and 7943 states for the $4lnl'$, $5lnl'$, and $3d4l'4l''nl$ autoionizing states to obtain the results shown in curve 4 in bottom right panel of Fig. 2. The dependence of the present results on the upper limit of n was also investigated. We found that there is a small difference for low temperature (4% for T$_e$ = 100 eV) with $n=20$ instead of $n=100$ as the upper limit for $3d4l'4l''nl$ autoionizing states; the difference increases for

high temperatures, reaching 7% for T_e = 1 keV.

The high-n state contributions are very important for high temperatures. One can see from Fig. 2 that for $T_e >$ 1 keV, the curves 4 describing the scaled contributions from the high-n states ($4l'nl$ states with n=13-1000, $5l'nl$ states with n=9-500, and $3d4l'4l''nl$ states with n=6-100) are above curves 1, 2, and 3 for three panels ($3d^{10}4s5p$, $3d^{10}4d5s$, and $3d^{10}4p5p$ states), shown on Fig. 2. The scaling contribution (curve 4) is above the curves 2 and 3; however, it is below curve 2 for the $3d^{10}4d5s$ states (top, right panel of Fig. 2). The sum of the contributions presented by the curves 1, 2, 3, and 4 gives the DR rate coefficients for excited states.

In Fig. 3, we show the contribution of the scaled terms. The three curves presented in Fig. 3 illustrate the contributions from the sum of the $3d^{10}[4l_1 4l - 4l_2 nl]$ transitions with n = 13-1000, the sum of the $3d^{10}[4l_1 5l - 5l_2 nl]$ with n = 9-1000, and the sum of the $3d^{10}4_1 4l - 3d^9 4l_2 4l_3 nl$ transitions with n = 6-500 to the total DR rate coefficient $\alpha_d(4s)$ as a function of l and T_e in Zn-like tungsten. It should be noted that we observed a large mixing between configurations. For example, the dipole one-electron $4s4d - 4d12p$, $4d^2 - 4d12p$ transitions were found to interact strongly with the $4f^2 - 4d12p$, $4s^2 - 4d12p$ two-electron transitions. In other words, we found strong mixing between the $4s4d$, $4d^2$, $4f^2$, and $4s^2$ configurations.

The calculated values of $\alpha_d(3d^{10}4s, j)$ are presented in Fig. 4 as function of T_e. Here j corresponds to the even-parity states $3d^{10}4l^2$, $3d^{10}4p4f$, $3d^{10}4s4d$, $3d^{10}4s5l_1$, $3d^{10}4d5l_1$, $3d^{10}4p5l_2$, $3d^{10}4f5l_2$ ($l_1 = s, d, g$ and $l_2 = p, f$), $3d^9 4s^2 4d$, and $3d^9 4p^2 4d$ as function of T_e in Zn-like W. Values of $\alpha_d(3d^{10}4s, j)$ where j corresponds to odd-parity states ($3d^{10}4s4p$, $3d^{10}4s4f$, $3d^{10}4p4d$, $3d^{10}4s5l_1$, $3d^{10}4d5l_1$, $3d^{10}4p5l_2$, $3d^{10}4f5l_2$ ($l_1 = p, f$ and $2_1 = s, d, g$), $3d^9 4s^2 4p$, $3d^9 4p^3$, and $3d^9 4s4p4d$) are illustrated by Fig. 5. Finally, the values of the DR rate coefficient $\alpha_d(3d^{10}, j)$ for $j = 3d^{10}5l^2$ ($l = s, p, d$), $3d^{10}5s5d$, $3d^{10}5p5f$, $3d^{10}5s5p$, $3d^{10}5s5f$, $3d^{10}5p5d$, and $3d^{10}5d5f$ states are shown as function of T_e in two panels of Fig. 6. The electron temperature for these plots varies from T_e=0.1 eV to T_e=38.3 keV.

As can be seen from Figs. 4 - 6, the DR rate coefficients can be divided into three different groups based on the variation with electron temperature. There are curves without any maximum such as, e.g., $\alpha_d(3d^{10}4s, j)$ for j = $3d^{10}4s4d$ (Fig. 4) and $3d^9 4p^3$ (Fig. 5). Then, there are curves with two maxima: j= $3d^{10}4s5d$ (bottom, left panel of Fig. 4)(at about 5.12 eV and 442 eV) and j= $3d^{10}4s5f$ (top, right panel of Fig. 5)(at about 3.03 eV and 340 eV). The largest group of DR rate coefficients exhibits only one maximum around 2.0 eV to 5 eV.

Among states with one maximum , the largest values (10^{-11} in units of cm^3/s) for the DR rate coefficient $\alpha_d(3d^{10}4s, j)$ are found for j= $3d^{10}4d^2$ at 5.12 eV (top left panel of Fig. 4), for j= $3d^{10}4p4f$ at 5.12 eV (top right panel of Fig. 4), for j= $3d^{10}4p5f$ at 5.12 eV (bottom right panel of Fig. 4), for j= $3d^{10}4p4d$ at 3.03 eV (top left panel of Fig. 5), and for j= $3d^{10}4d5f$ at 2.33 eV (bottom right panel of Fig. 5).

One can see from the left panel of Fig. 6 that DR rate coefficients on these states exhibit only one maximum around 54 eV to 201 eV. The largest value (3.69×10^{-13} in units of cm^3/s) of the DR rate coefficients $\alpha_d(3d^{10}4s, j)$ among the even-parity $3d^{10}5l5l'$ states with one maximum is obtained for states with j= $3d^{10}5p5f$ at 201 eV (curve 5). Such a relatively small value for the DR rate coefficients $\alpha_d(3d^{10}4s, j)$ with $j = 3d^{10}5l5l'$ is caused by the small number of transitions between these states and autoionising states. For example, only 1731 transitions are involved in creating curve 5 describing the DR rate coefficient for the $3d^{10}5p5f$ state, while there are 13716 transitions involved in creating curve 1 (top right panel of Fig. 4 describing the DR rate coefficient for the $3d^{10}4p4f$ state with a maximum at 3.96×10^{-11} in units of cm^3/s).

V. TOTAL DIELECTRONIC RECOMBINATION RATE COEFFICIENTS

The total DR rate coefficients are obtained by the summation of the effective emission rate coefficients $C_S^{eff}(j, i)$ (Eq. (3)) over all possible intermediate singly and doubly excited states:

$$\alpha_d(i_0) = \sum_i \sum_j C_S^{eff}(j, i). \qquad (5)$$

We have already discussed the contribution from doubly excited and core-excited states with high-n levels to the DR rate coefficients (sum over i in Eq. (4)). For the total DR rate coefficients one has to consider also the contribution from singly excited high-n states, i.e., the $4snl$ states. For these states, the most important transitions are $4snl - 4pnl$ and $4snl - 5pnl$ [23, 68]. Including the core-excited states creates more channels for transitions from singly excited high-n states, such as the $3d^{10}4snl - 3d^9 4s4pnl$ channels.

To estimate $Q_d(j, i)$ in Eq. (2) with $j = 3d^{10}4snl$ and $i = 3d^{10}4pnl$ for $n > 12$, we used the calculated data for n = 12 and the $1/n^3$ scaling law for A_a and E_S. The values of A_r for the $3d^{10}4snl - 3d^{10}4pnl$ transitions are almost independent of n since this is a one-electron $4s-4p$ transition (see Ref. [23, 68] for details.

Again, the calculated data for n = 12 and the $1/n^3$ scaling law for A_a were used for estimates of $Q_d(j, i)$ in Eq.(2) for autoionization states i with high n. For the $3d^{10}4snl - 3d^{10}4pnl$ transitions, the scaling begins from n = 12. Using the scaling formulas for $A_r\left(3d^{10}4snl^{1,3}L'_{J'} - 3d^{10}4pnl\ ^{1,3}L_J\right)$ and $A_a(3d^{10}4pnl\ ^{1,3}L_J)$, we calculated $Q_d(3d^{10}4snl^{1,3}L'_{J'} - 3d^{10}4pnl\ ^{1,3}L_J)$ and then, using screened value of E_S [23, 68], we calculated $C_S^{\rm eff}(3d^{10}4snl^{1,3}L'_{J'} - 3d^{10}4pnl\ ^{1,3}L_J)$. The sums over LSJ and for $C_S^{\rm eff}(3d^{10}4snl^{1,3}L'_{J'} - 3d^{10}4pnl\ ^{1,3}L_J)$ give data for $C_S^{\rm eff}(3d^{10}4snl - 3d^{10}34pnl)$ as a function of nl and T_e.

The results of the calculations for $C_S^{\rm eff}(3d^{10}4snl - 3d^{10}4pnl)$ are illustrated in Fig. 7 for the $3d^{10}4snf - 3d^{10}4pnf$ and $3d^{10}4sng - 3d^{10}4png$ transitions. In Fig. 7, we show the contribution from the scaled data for n = 13 to n = 1000 (curves 1). The contributions from the $3d^{10}4snl - 3d^{10}5pnl$ and $3d^{10}4snl - 3d^{9}4s4pnl$ ($l = f, g$) transitions are shown by curves 2 and 3, respectively. We already mentioned that the scaling for the $5lnl'$ and $3d^{9}4s4pnl$ states is started from $n = 9$ and $n = 5$, respectively. One can see from these plots that the largest contributions at low temperature T_e=41.7 eV and 70.6 eV come from the $3d^{10}4snf - 3d^{10}4pnf$ and $3d^{10}4sng - 3d^{10}4png$ scaling, respectively. The maximum values are equal to about 1.57×10^{-13} and 4.90×10^{-12} cm^3/s, respectively on the left and right panels of Fig. 7. The contribution from the scaled data for n = 13 to n = 1000 is illustrates by curve 1. The contributions from the $3d^{10}4snl - 3d^{10}5pnl$ and $3d^{10}4snl - 3d^{9}4s4pnl$ ($l = f, g$), shown by curves 2 and 3, are important at high T_e (the maximum value is reached at 576 eV).

The final result for the sum of the $3d^{10}4snl - 3d^{9}4pnl$, $3d^{10}4snl - 3d^{10}5pnl$, and $3d^{10}4snl - 3d^{10}4s4l'nl$ contributions from high-n states to the total DR rate coefficient $\alpha_d(3d^{10}4s)$ is shown in Fig. 8. In this figure, the values of the sum of $\sum_{n=13}^{n=1000} C_S^{eff} 3d^{10}[4snl - 4pnl] + \sum_{n=9}^{n=1000} C_S^{eff} 3d^{10}[4snl - 5pnl] + \sum_{n=6}^{n=500} C_S^{eff}(3d^{10}4snl - 3d^{9}4s4l'nl)$ is presented as a function of T$_e$ for different values of l. The largest contribution is obtained from the sum of $[\sum_{n=13}^{n=1000} C_S^{eff} 3d^{10}[4snl - 4pnl]$ for most of the cases.

We used nl names (where $l = s$, p, d, f, g, h, i, and k) to label the curves in Fig. 8. The largest and smallest scaling contribution illustrated by Fig. 8 changes with with temperature. The largest contribution to the first maximum (at 70.6 eV) is obtained from values of the sum with $l = 6$ (ni curve). A somewhat smaller contribution comes from the sum with $l = 4$ (ng curve). The smallest contribution is from the $l = 2$ sum (nd curve). The largest contribution to the second maximum (at 576 eV) is obtained from the sum with $l = 4$ (ng curve), followed by a contribution from the sum with $l = 6$ (ni curve). The smallest contribution to the peak is from the sum with $l = 7$ (nk curve). As can be seen from the labels in Fig. 8, that the order of contributions changes again at largest T$_e$. In this case, the largest contribution comes from the sum with $l = 3$ (nf curve).

The total DR rate coefficient ($\alpha_d^{\rm tot}$ in cm^3/s) is calculated as a sum of five terms: α_d^{44}, α_d^{45}, α_d^{34}, $\alpha_d^{\rm scale1}$, and $\alpha_d^{\rm scale2}$. The contributions of α_d^{44}, α_d^{45}, and α_d^{34} are the sums over the $3d^{10}4l_1n_2l_2 - 3d^{10}4l'nl$ transitions with n=4-12, the $3d^{10}4l_1n_2l_2 - 3d^{10}5l'nl$ transitions with n=4-8, and the $3d^{10}4l_1n_2l_2 - 3d^{9}4l'4l''nl$ transitions with n=4-5, respectively.

The term α_d^{scale1} is the contribution from the high-n states for transitions from the sum of the transitions $3d^{10}[4l_14l - 4l_2nl]$ with n = 13-1000, $3d^{10}[4l_15l - 5l_2nl]$ with n = 9-1000, and $3d^{10}4l_14l - 3d^{9}4l_24l_3nl$ with n = 6-500. The term α_d^{scale2} is evaluated from the sum of three contributions: $\sum_{n=13}^{n=1000} C_S^{eff}(3d^{10}[4snl - 4pnl])$, $\sum_{n=8}^{n=1000} C_S^{eff}(3d^{10}[4snl - 5pnl])$, and $\sum_{n=6}^{n=500} C_S^{eff}(3d^{10}4snl - 3d^{9}4s4l'nl)$.

The results for α_d^{44}, α_d^{45}, α_d^{34}, $\alpha_d^{\rm scale1}$, and $\alpha_d^{\rm scale2}$ are shown by curves 1, 2, 3, 4, and 5 in Fig. 9. The electron temperature for these plots varies from 0.1 eV to 38.3 keV. It is clearly seen that α_d^{44} gives the dominant contribution for low T$_e$ from 0.48 eV up to 90 eV and has a maximum at 3.9 eV, while α_d^{34} dominates for the lowest temperature (0.10 eV - 0.48 eV). That contribution (curve 3) dominates also at larger temperatures (about 570 eV), but at even higher temperatures the scaled term (curve 4, $\alpha_d^{\rm scale1}$) becomes more important term.

Values of the total rate coefficient $\alpha_d^{\rm total}$ are presented in Table VII for T$_e$ = 0.1 eV to 30.3 keV on a logarithmic grid $T_e = (0.1 \times 1.3^{N-1})$ eV with N = 1–50.

VI. UNCERTAINTY ESTIMATES AND CONCLUSION

In the present paper we calculated a large set of atomic data related to the dielectronic recombination of Cu-like W into Zn-like W^{44+}.

Energy levels, wavelengths, weighted radiative transition probabilities, and autoionization rates were calculated for the Zn-like tungsten ion using three theoretical methods. To check the accuracy of our results obtained by the Cowan code, we evaluated energies, wavelengths and transition rates by including two-electron states as well as core-excited state using the multi-configuration relativistic HULLAC code, in addition, the relativistic many-body perturbation theory method was used to evaluate energies of two-electron states. The calculated atomic data were used to obtain the dielectronic satellite lines as well as the DR rate coefficients.

The energies calculated by the Cowan code are in a good agreement with the second-order RMBPT energies, because the largest portion of the correlation contribution is taken into account by the atomic structure code of Cowan [61] by scaling the electrostatic integrals. The accuracy of the transition rates is estimated to be about 20-50% for the largest gA_r values and within a factor of 2-5 for the smallest ones. Such large differences are due to substantial contribution of correlation effects not fully accounted by the Cowan code [61]. The accuracy of the autoionizing rates gA_a is about 20-40% for the largest values of gA_a ($gAa \simeq 10^{13}$-10^{14} s^{-1}).

Energies of the $3d^{9}4l4l'4l$" core-excited states of Zn-like tungsten, obtained using COWAN and HULLAC codes, are compared with values compiled by NIST [56]. Excellent agreement (0.1% - 0.4%) is observed for the energies the $3d^{9}4l4l'4l$" core-excited states. This agreement is even better than that demonstrated for two-electron excited states. The difference between the NIST values and the COWAN and HULLAC values computed for the two-electron excited states is less than 0.4% and 0.5%,

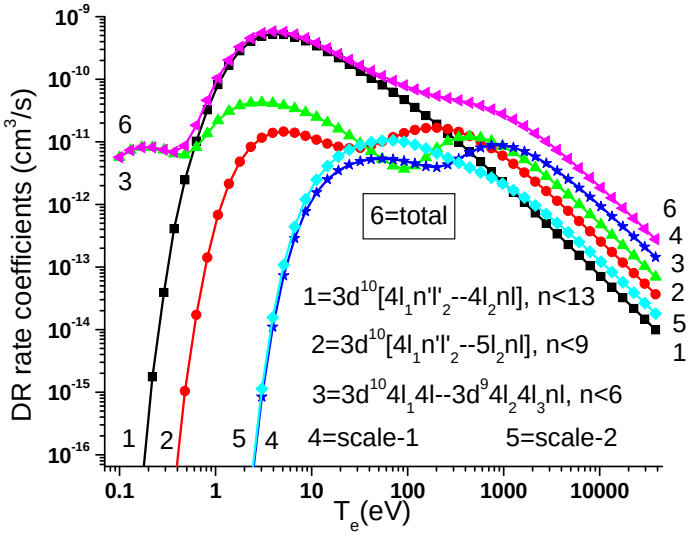

FIG. 9: (Color online) Total DR rate coefficient ($\alpha_d^{\rm total}$) as a function of T_e in Zn-like tungsten. "Scale-1" describes the contribution from the high-n states for transitions from the $3d^{10}4l4l'$ and $3d^{10}4l5l'$ states to the $3d^{10}4lnl'$ states with n=13-1000, $3d^{10}5lnl'$ states with n=9-1000, and $3d^94l4l'nl_1$ states with n=5-1000. "Scale-2" describes the sum of the three contributions: $\sum_{n=13}^{n=1000} C_S^{eff}(3d^{10}4snl - 3d^{10}5pnl)$, $\sum_{n=9}^{n=1000} C_S^{eff}(3d^{10}4snl - 3d^{10}5pnl)$, and $\sum_{n=6}^{n=500} C_S^{eff}(3d^{10}4snl - 3d^94s4l'nl)$.

respectively. The comparison of NIST values and energies computed by the COWAN and HULLAC codes, thus, confirmed the high accuracy of our calculations.

We took into account the excited states [Ar]$3d^{10}4l'nl$ (n=4-12, $l \le n-1$), [Ar]$3d^{10}5l'nl$ (n=5-8, $l \le n-1$), and [Ar]$3d^94l'4l''nl$ (n=4-5, $l \le n-1$) states in Zn-like tungsten (W^{44+}) as intermediate resonance states with n up to 1000 to calculate the DR rate coefficients. Most of the state-selective DR rate coefficients reveal a double peak as a function of electron temperature. The $3d^{10}[4l_1n_2l_2 - 4l'nl]$ transitions with n=4-12 give the dominant contribution for T_e from 0.48 eV up to 90 eV, while the $3d^{10}4l_1n_2l_2 - 3d^94l'4l''nl$) transitions dominate at the lowest temperature (0.48 eV). The scaled term (that takes case of the contributions from states involving a high n electrons) becomes more important with increasing temperature.

The state selective rate coefficients can be used in collisional-radiative models aimed at investigating the population kinetics in recombining plasmas as well as in the calculation of ionization equilibrium. In addition, the spectra of the dielectronic satellites of W^{44+} are important as a diagnostic of high-temperature L-shell W plasmas in general, and of future ITER plasmas in particular.

TABLE VII: Total DR rate coefficients $\alpha_d^{\rm total}$ (in cm^3/s) for different temperature values. A[B] means A·10^B.

T_e (eV)	$\alpha_d^{\rm total}$	T_e (eV)	$\alpha_d^{\rm total}$
0.10	5.66[-12]	70.56	9.39[-11]
0.13	7.35[-12]	91.73	7.97[-11]
0.17	8.21[-12]	119.25	6.87[-11]
0.22	8.16[-12]	155.03	6.04[-11]
0.29	7.48[-12]	201.54	5.43[-11]
0.37	6.90[-12]	262.00	4.98[-11]
0.48	8.69[-12]	340.60	4.59[-11]
0.63	1.84[-11]	442.78	4.21[-11]
0.82	4.62[-11]	575.61	3.78[-11]
1.06	1.05[-10]	748.30	3.30[-11]
1.38	2.02[-10]	972.78	2.78[-11]
1.79	3.27[-10]	1264.62	2.26[-11]
2.33	4.53[-10]	1644.01	1.78[-11]
3.03	5.44[-10]	2137.21	1.36[-11]
3.94	5.83[-10]	2778.37	1.02[-11]
5.12	5.70[-10]	3611.88	7.43[-12]
6.65	5.20[-10]	4695.44	5.34[-12]
8.65	4.52[-10]	6104.07	3.78[-12]
11.25	3.80[-10]	7935.30	2.65[-12]
14.62	3.12[-10]	10315.89	1.84[-12]
19.00	2.53[-10]	13410.65	1.27[-12]
24.71	2.04[-10]	17433.84	8.73[-13]
32.12	1.65[-10]	22664.00	5.97[-13]
41.75	1.35[-10]	29463.19	4.07[-13]
54.28	1.12[-10]	38302.15	2.77[-13]

Acknowledgments

This work was supported in part by DOE under NNSA Cooperative Agreement DE-NA0001984. Work at LLNL was performed under auspices of the US DOE under Contract No. DE-AC52- 07NA-27344.

[1] K. Spruck, N. R. Badnell, C. Krantz, O. Novotný, A. Becker, D. Bernhardt, M. Grieser, M. Hahn, R. Repnow, D. W. Savin, et al., Phys. Rev. A **90**, 032715 (2014).
[2] P. Beiersdorfer, M. J. May, J. H. Scofield, and S. B. Hansen, High Energy Density Physics **8**, 271 (2012).
[3] H.-K. Chung, C. Bowen, C. J. Fontes, S. B. Hansen, and Yu. Ralchenko, High Energy Density Physics **9**, 645 (2013).
[4] Stephanie Hansen, G. S. J. Armstrong, S. Bastiani-Ceccotti, C. Bowend, H. J. P. Colgan, F. de Dortan, C. J. Fontes, F. Gilleron, and J.-R. Marqus, High Energy Density Physics **9**, 523 (2013).

[5] P. Beiersdorfer, J. Phys. B **48**, in press (2015).
[6] P. Beiersdorfer, J. Clementson, K. Widmann, M. Bitter, K.-W. Hill, D. Johnson, R. Barnsley, H.-K. Chung, and U. I. Safronova, AIP Conf. Proc. p. in press (2015).
[7] P. Beiersdorfer, J. Clementson, K. Widmann, M. Bitter, K.-W. Hill, D. Johnson, R. Barnsley, H.-K. Chung, and U. I. Safronova, J. Phys. B **43**, 144008 (2010).
[8] C. R. Seon, S. H. Choi, M. S. Cheon, S. Pak, H. G. Lee, W. Biel, and R. Barnsley, Rev. Scient. Instr. **81**, 10E508 (2010).
[9] S. K. Varshney, R. Barnsley, M. G. OMullane, and S. Jakhar, Rev. Scient. Instr. **83**, 10E126 (2012).
[10] L. I. Maijuan, F. U. Yanbiao, S. U. Maogen, DONG Chenzhong, and Koike FUMIHIRO, Plasma Science and Technology **16**, 182 (2014).
[11] M. J. Li, Y. B. Fu, G. D. Zhang, Y. Z. Zhang, C. Z. Dong, and F. Koike, J. Phys. Conf. Series **488**, 062022 (2014).
[12] L. Xie, X. Ma, C. Dong, Z. Wu, Y. Shi, and J. Jiang, J. Quant. Spect. Rad. Transfer **141**, 31 (2012).
[13] S. Schippers, D. Bernhardt, A. Müller, C. Krantz, M. Grieser, R. Repnow, A. Wolf, M. Lestinsky, M. Hahn, O. Novotný, et al., Phys. Rev. A **83**, 012711 (2011).
[14] S. Schippers, D. Bernhardt, A. Müller, C. Krantz, M. Grieser, R. Repnow, A. Wolf, M. Lestinsky, M. Hahn, O. Novotný, et al., J. Phys: Conf. Series **388**, 062028 (2012).
[15] N. R. Badnell, C. P. Ballance, D. C. Griffin, and M. OMullane, Phys. Rev. A **85**, 052716 (2012).
[16] V. A. Dzuba, V. V. Flambaum, G. F. Gribakin, , and C. Harabati, Phys. Rev. A **86**, 022714 (2012).
[17] B. W. Li, G. O'Sullivan, Y. B. Fu, and C. Z. Dong, Phys. Rev. A **85**, 052706 (2012).
[18] U. I. Safronova and A. S. Safronova, Phys. Rev. A **85**, 032507 (2012).
[19] U. I. Safronova, A. S. Safronova, and P. Beiersdorfer, Phys. Rev. A **86**, 042510 (2012).
[20] U. I. Safronova, A. S. Safronova, and P. Beiersdorfer, J. Phys. B **45**, 085001 (2012).
[21] U. I. Safronova, A. S. Safronova, P. Beiersdorfer, and W. R. Johnson, J. Phys. B **44**, 035005 (2011).
[22] U. I. Safronova, A. S. Safronova, and P. Beiersdorfer, At. Data Nucl. Data Tab. **95**, 751 (2009).
[23] U. I. Safronova, A. S. Safronova, and P. Beiersdorfer, J. Phys. B **42**, 165010 (2009).
[24] U. I. Safronova, A. S. Safronova, and P. Beiersdorfer, Can. J. Phys. **89**, 581 (2011).
[25] E. Behar, A. Peleg, R. Doron, P. Mandelbaum, and J. L. Schwob, J. Quant. Spectrosc. Radiat. Transf. **58**, 449 (1997).
[26] E. Behar, R. Doron, P. Mandelbaum, and J. L. Schwob, Phys. Rev. A **58**, 2115 (1998).
[27] A. Peleg, E. Behar, P. Mandelbaum, and J. L. Schwob, Phys. Rev. A **57**, 3493 (1998).
[28] E. Behar, P. Mandelbaum, and J. L. Schwob, Eur. Phys. J. D **7**, 157 (1999).
[29] E. Behar, P. Mandelbaum, and J. L. Schwob, Phys. Rev. A **59**, 2787 (1999).
[30] E. Behar, R. Doron, P. Mandelbaum, and J. L. Schwob, Phys. Rev. A **61**, 062708 (2000).
[31] Fan-Chang Meng, Chong-Yang Chen, Yan-Sen Wang, and Ya-Ming Zou, J. Quant. Spectrosc. Radiat. Transf. **109**, 2000 (2008).
[32] Fan-Chang Meng, Li Zhou, Min Huang, Chong-Yang Chen, Yan-Sen Wang, and Ya-Ming Zou, J. Phys. B **42**, 105203 (2009).
[33] C. P. Ballance, S. D. Loch, M. S. Pindzola, and D. C. Griffin, J. Phys. B **43**, 205201 (2010).
[34] J. Clementson, P. Beiersdorfer, T. Brage, and M. F. Gu, At. Data Nucl. Data Tables **100**, 577 (2014).
[35] S. Spencer, A. Hibbert, and C. A. Ramsbottom, J. Phys. B **47**, 245001 (2014).
[36] T. Das, L. Sharma, and R. Srivastava, Phys. Scr. **86**, 035301 (2012).
[37] F. Hu, G. Jiang, J. M. Yang, C. K. Wang, X. F. Zhao, and L. H. Hao, Eur. Phys. J. D **61**, 15 (2011).
[38] G. C. Osborne, A. S. Safronova, V. L. Kantsyrev, U. I. Safronova, K. M. Williamson, M. E. Weller, and I. Shrestha., Can. J. Phys. **89**, 599 (2011).
[39] U. I. Safronova and A. S. Safronova, J. Phys. B **43**, 074026 (2010).
[40] U. I. Safronova and M. S. Safronova, J. Phys. B **43**, 074025 (2010).
[41] M. H. Chen and K. T. Cheng, J. Phys. B **43**, 074019 (2010).
[42] S. A. Blundell, W. R. Johnson, M. S. Safronova, , and U. I. Safronova, Phys. Rev. A **77**, 032507 (2008).
[43] P. Quinet, E. Biémont, P. Palmeri, and E. Träbert, At. Data Nucl. Data Tables **93**, 711 (2007).
[44] Y. Ralchenko, J. Reader, J. M. Pomeroy, J. N. Tan, and J. D. Gillaspy, J. Phys. B **40**, 3861 (2007).
[45] U. I. Safronova, Mol. Phys. **98**, 1213 (2000).
[46] K. B. Fournier, At. Data Nucl. Data Tables **68**, 1 (1998).
[47] T.-C. Cheng and K.-N. Huang, Phys. Rev. A **45**, 4367 (1992).
[48] L. J. Curtis, J. Opt. Soc. Am. B **9**, 5 (1992).
[49] E. Biémont, At. Data Nucl. Data Tables **43**, 163 (1989).
[50] E. Biemont and M. Godefroid, Phys. Scr. **22**, 231 (1980).
[51] C. F. Fischer and J. E. Hansen, Phys. Rev. A **19**, 1819 (1979).
[52] S. M. Younger and W. L. Wiese, Phys. Rev. A **18**, 2366 (1978).
[53] P. Shorer, Phys. Rev. A **18**, 1060 (1978).
[54] C. F. Fischer and J. E. Hansen, Phys. Rev. A **17**, 1956 (1978).
[55] P. Shorer and A. Dalgarno, Phys. Rev. A **16**, 1502 (1977).
[56] A. E. Kramida and T. Shirai, At. Data and Nucl. Data Tables **95**, 305 (2009).
[57] R. D. Cowan, Informal, Los Alamos Scientific Lab., Univ. California, Los Alamos (1977).
[58] A. Bar-Shalom, M. Klapisch, and J. Oreg, J. Quant. Spectr. Radiat. Transfer **71**, 169 (2001).
[59] M. S. Safronova, W. R. Johnson, and U. I. Safronova, Phys. Rev. A **53**, 4036 (1996).
[60] U. I. Safronova, W. R. Johnson, M. S. Safronova, and A. Derevianko, Phys. Scr. **59**, 286 (1999).
[61] URL `http://das101.isan.troitsk.ru/cowan.htm`.
[62] S. B. Utter, P. Beiersdorfer, and E. Träbert, Can. J. Phys. **80**, 1503 (2002).
[63] Yu. Ralchenko, J. Reader, J. M. Pomeroy, J. N. Tan, and J. D. Gillaspy, J. Phys. B **40**, 3861 (2007).
[64] L. A. Vainshtein and U. I. Safronova, At. Data and Nucl. Data Tables **21**, 49 (1978).
[65] J. Dubau and S. Volonte, Rep. Prog. Phys. **43**, 199 (1980).
[66] U. Safronova, A. Vasilyev, and R. Smith, Can. J. Phys. **78**, 1055 (2000).
[67] U. I. Safronova and T. Kato, J. Phys. B **31**, 2501 (1998).

[68] I. Murakami, T. Kato, D. Kato, U. I. Safronova, and Y. Ralchenko, J. Phys. B **39**, 1 (2006).